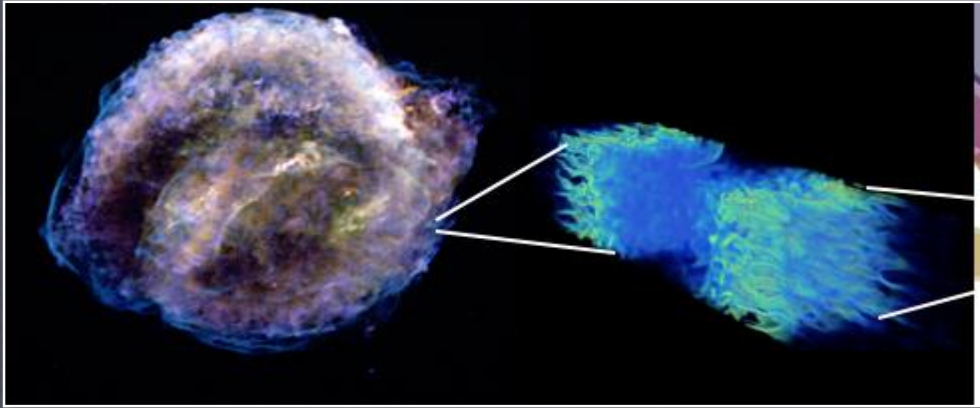

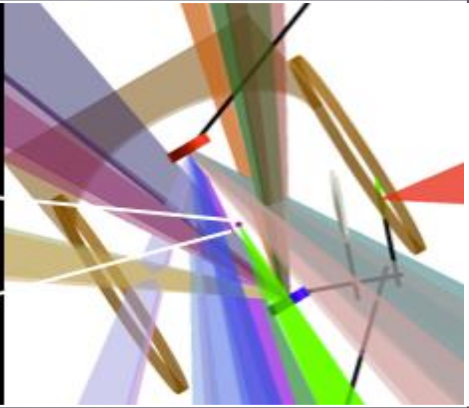

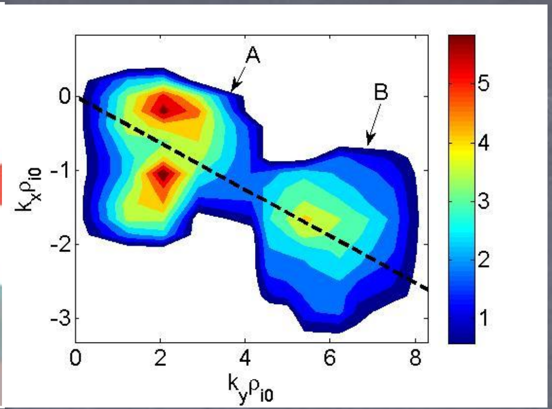

Astrophysical Collisionless Shocks and Current Sheet Instabilities: Results of Particle Modeling and Laboratory Study

Zhenyu Wang

Astrophysical Sciences, Princeton University

Shock collaborators: Anatoly Spitkovsky (Supervisor, Princeton), Channing. M. Huntington (LLNL), Hye-Sook Park (LLNL),

GeFi collaborators: Yu Lin (Auburn), X. Wang (Auburn), K. Tummel (UCI), Liu Chen (UCI)

Physics of Collisionless Shocks

Shock: sudden change in density, temperate, pressure that decelerates supersonic flow.
On earth: most of shocks are mediated by collision.

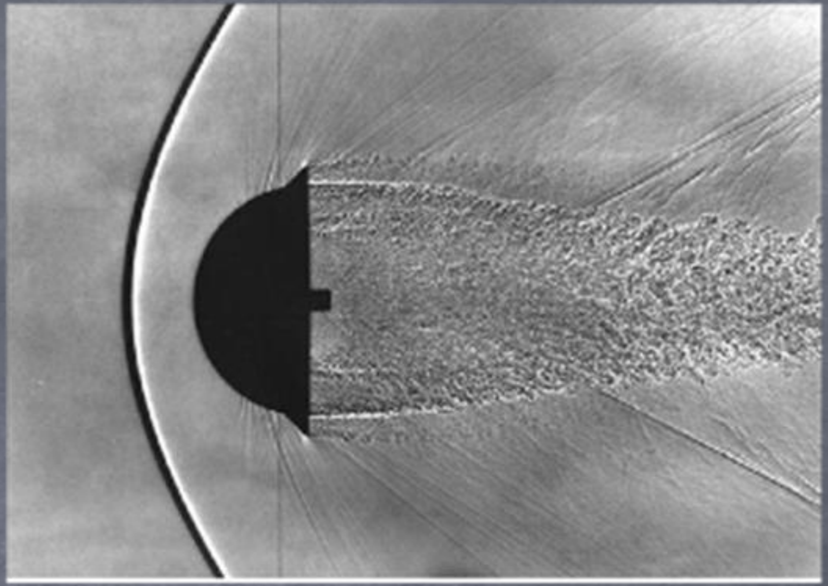

Collisionless:
Shocks must be mediated without direct collision, but through interaction with collective fields

Collisionless shocks are common in Astrophysics

Sources of particle acceleration, non-thermal emission, and magnetic fields amplification

PIC Simulation: A Powerful Tool for Studying Collisionless Shocks

Tristan-MP PIC code [Buneman 1991; Spitkovsky 2005]

Field Solver:

$$\nabla \times \boldsymbol{B} = \frac{4\pi}{c}\boldsymbol{J} + \frac{1}{c}\frac{\partial \boldsymbol{E}}{\partial t}$$

$$\nabla \times \boldsymbol{E} = -\frac{1}{c}\frac{\partial \boldsymbol{B}}{\partial t}$$

$\boldsymbol{E}, \boldsymbol{B}$

Field Interpolation:

$$\boldsymbol{F}_i = q_i\left(\boldsymbol{E}(r_i) + \frac{1}{c}\boldsymbol{v}_i \times \boldsymbol{B}\right)$$

Particle Push:

Non-relativistic: Boris Scheme

$$\boldsymbol{v}^- = \boldsymbol{v}^n + \frac{q}{m}\boldsymbol{E}^{n+\frac{1}{2}}$$

$\boldsymbol{v}^+$ = Rotation of $\boldsymbol{v}^-$ by $\boldsymbol{B}^{n+1/2}$

$$\boldsymbol{v}^{n+1} = \boldsymbol{v}^+ + \frac{q}{m}\boldsymbol{E}^{n+1/2}$$

Relativistic: Vay Scheme

$\boldsymbol{r}_i, \boldsymbol{v}_i$

Current Deposition:

$$\boldsymbol{J} = \Sigma q_i \boldsymbol{v}_i \mathrm{S}(\boldsymbol{r} - \boldsymbol{r}_i)$$

Charge Conservation: Zigzag/Esikepov

J

Tristan-MP is parallelized by MPI

Tristan-MP optimization: Multi-threads and Vectorization [Z. Wang, A. Spitkovsky]

80% computing time spend on particles, current deposition costs 60%.

Improve performance of current deposition is key!

Parallelize particles by OpenMP

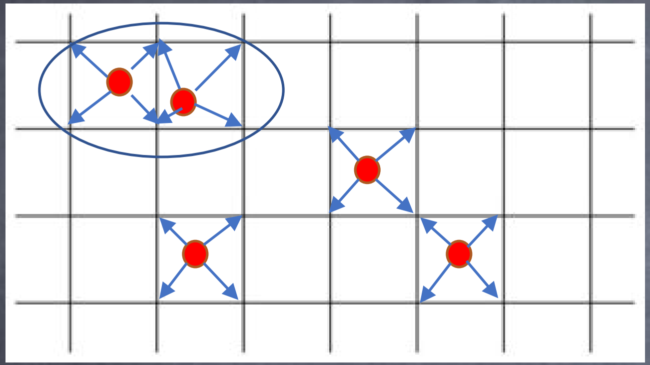

Data writing conflicts

use ATOMIC to prevent

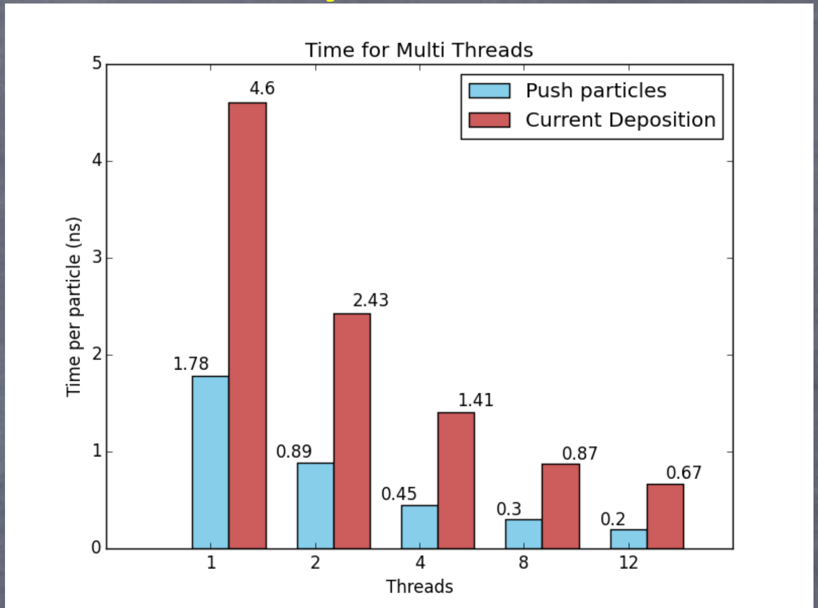

Good scaling for 2, 4, 8, 12 threads.

Vectorize Current Array Elements

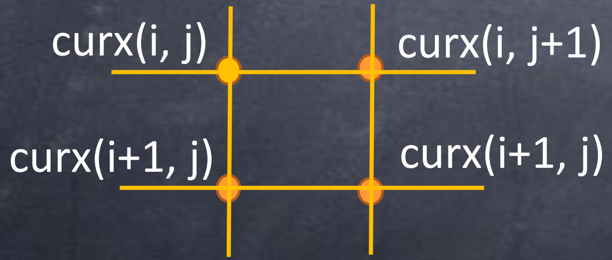

curx(i, j)	curx(i+1, j)

curx(i, j+1)	curx(i+1, j+1)

Reorder and vectorize the array elements

curx(j*ix+i+1)	curx(j*ix+i+2)	curx(j*ix+i+3)	curx(j*ix+i+4)

then using SIMD

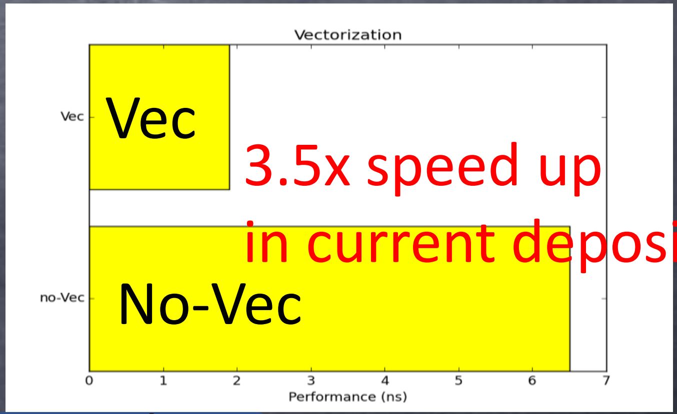

3.5x speed up in current deposition

How Collisionless Shocks Work

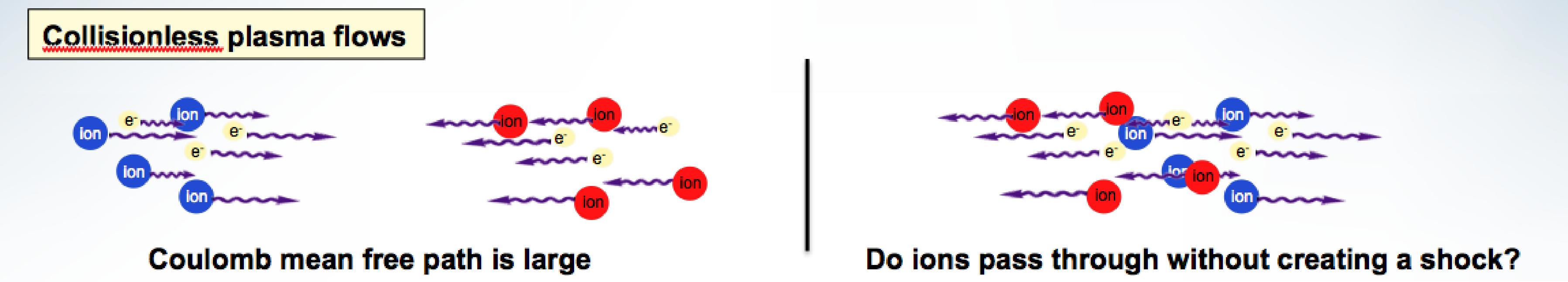

For low initial B field, particles are deflected by self-generated magnetic fields (filamentation/Weibel instability)

Experiment by laser: Fox et. al 2013, Huntington et. al 2015

For large initial B field, particles are deflected by compressed pre-existing fields

measurement of density compression through shadowgraphy (Schaeffer et. al 2017)

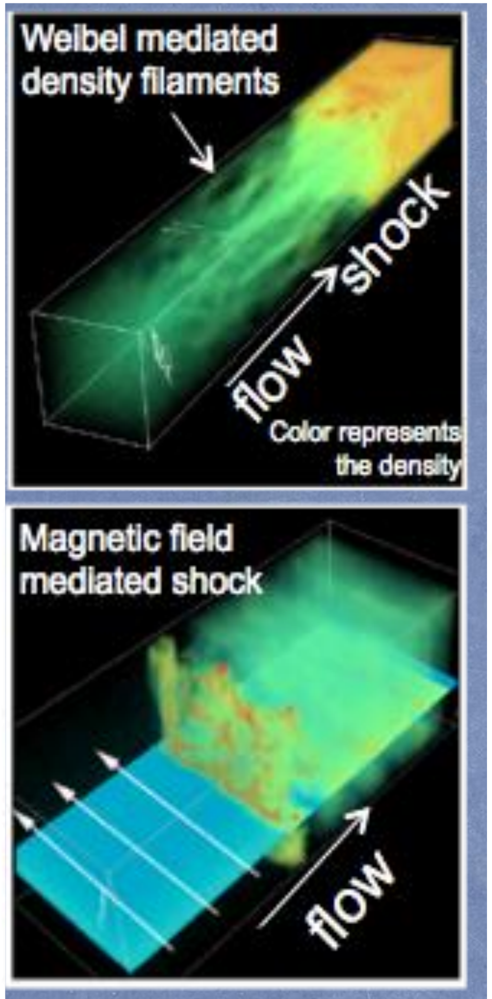

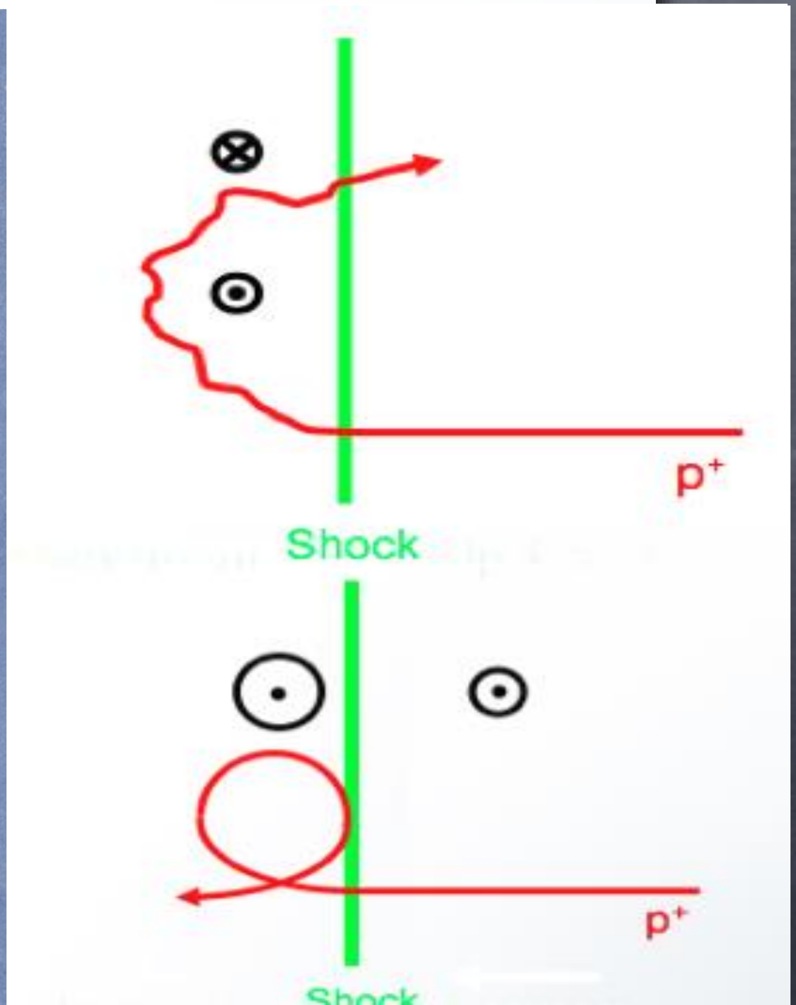

PIC Simulation of Unmagnetized Shock

[Spitkovsky, 2007]

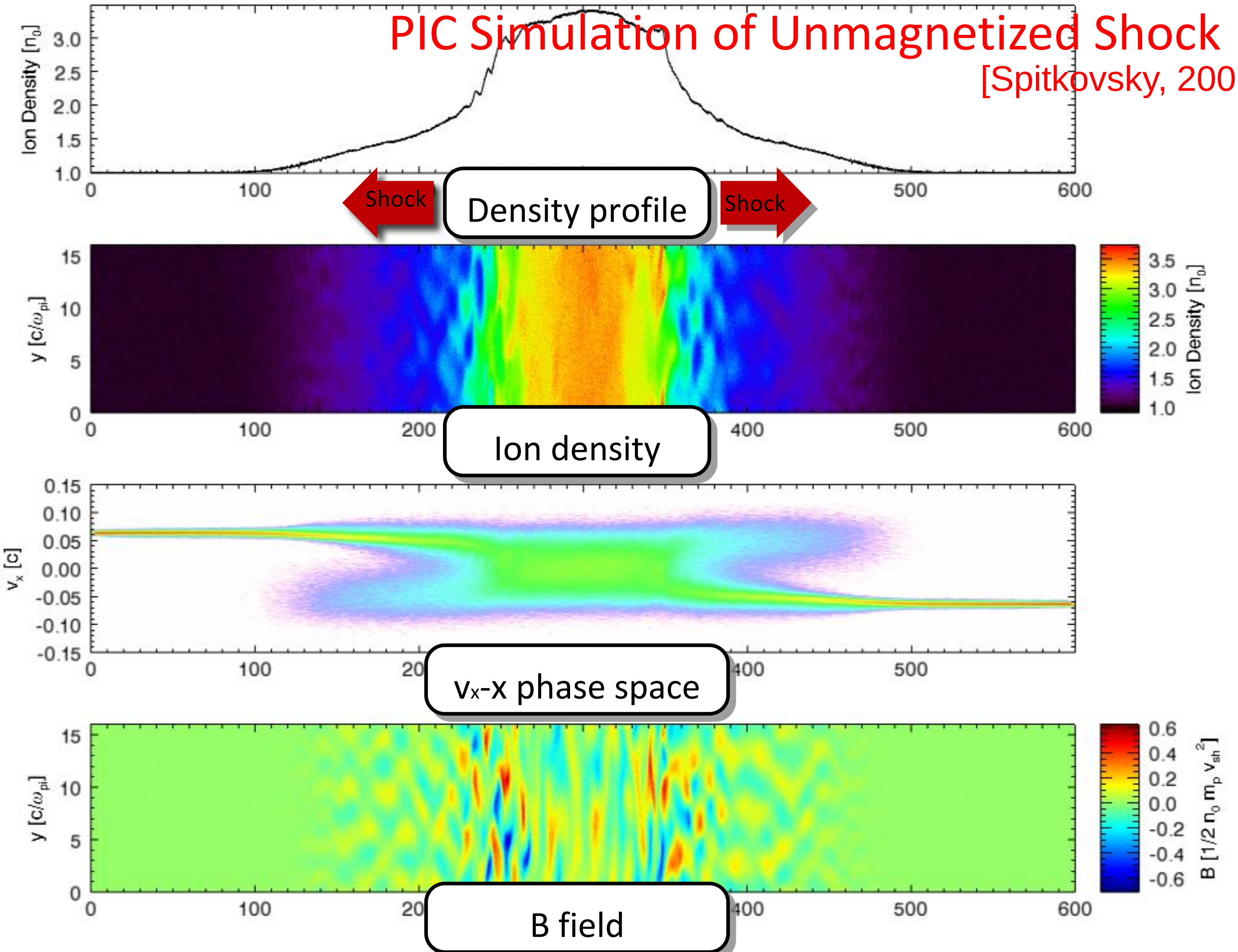

Magnetized Collisionless Shock

B field

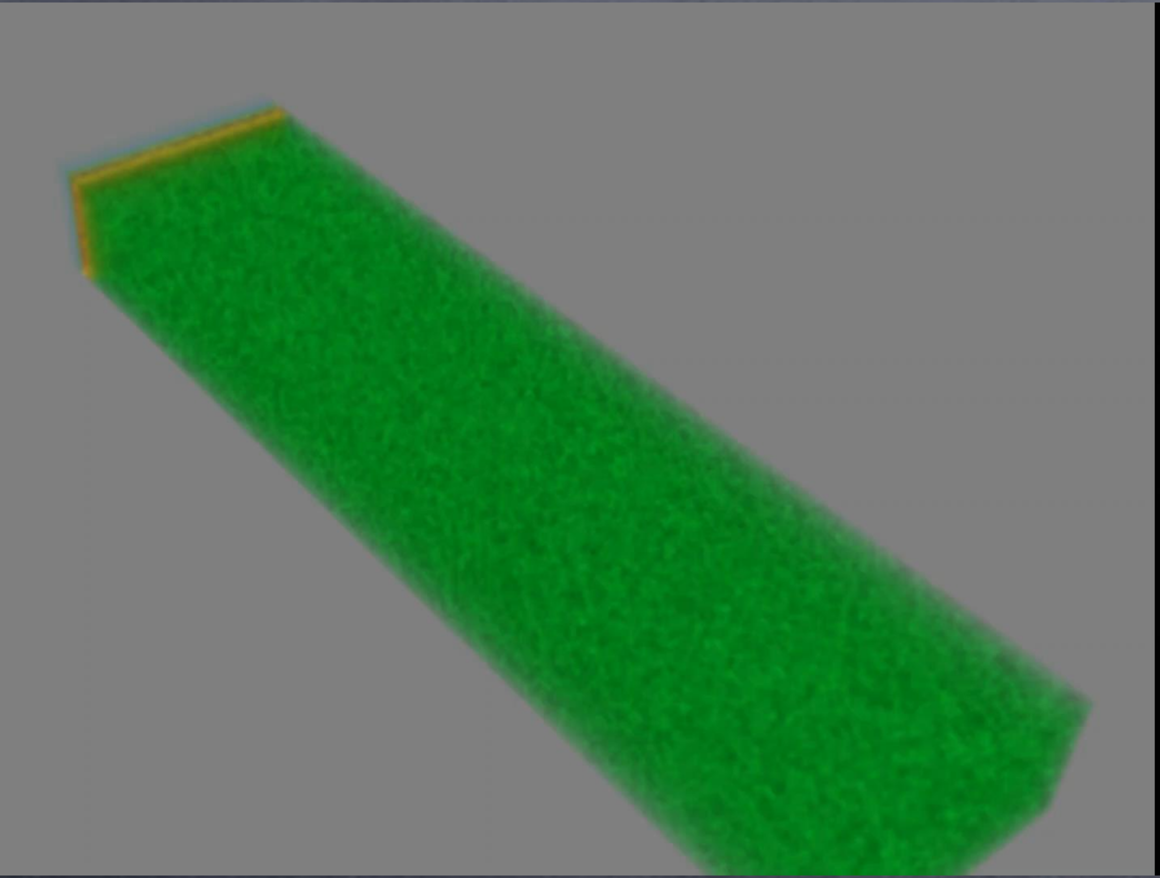

Density

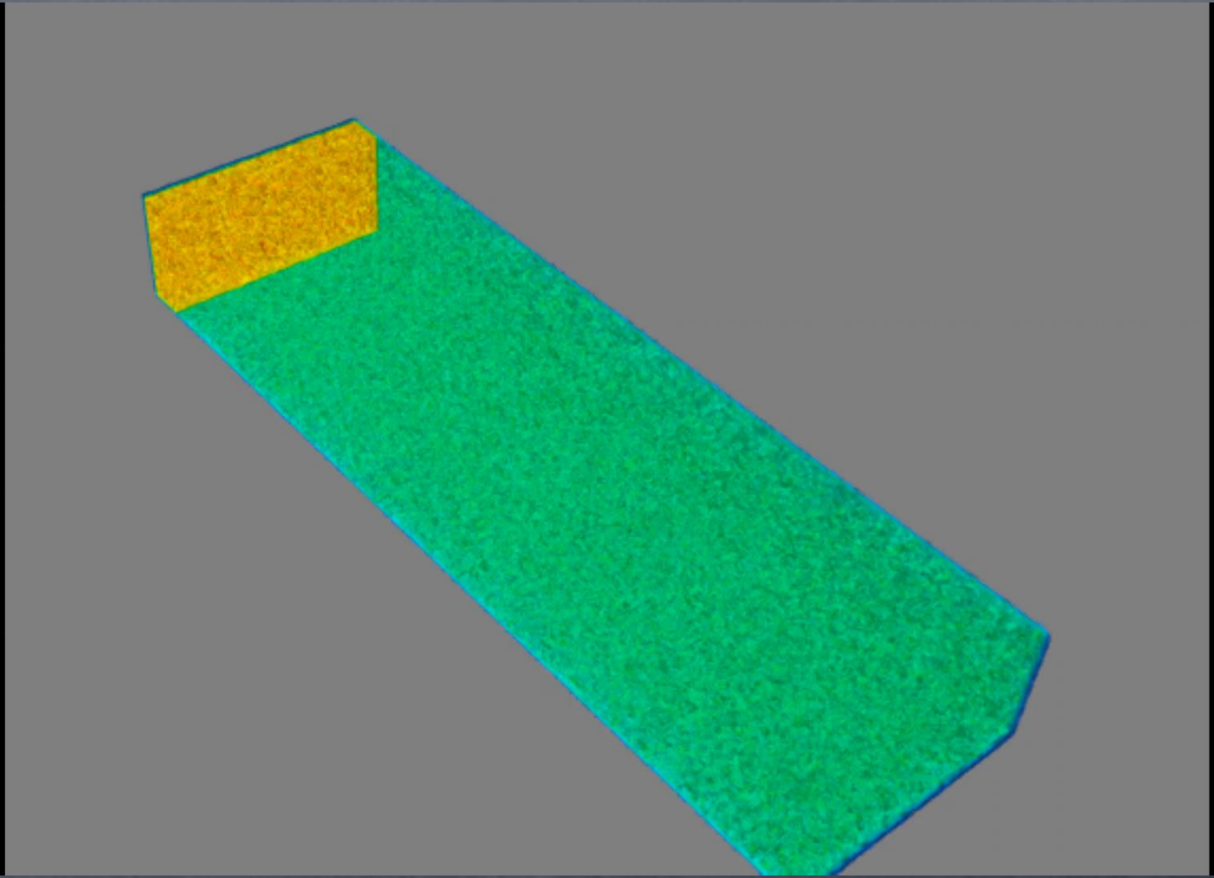

Formation of contact discontinuity

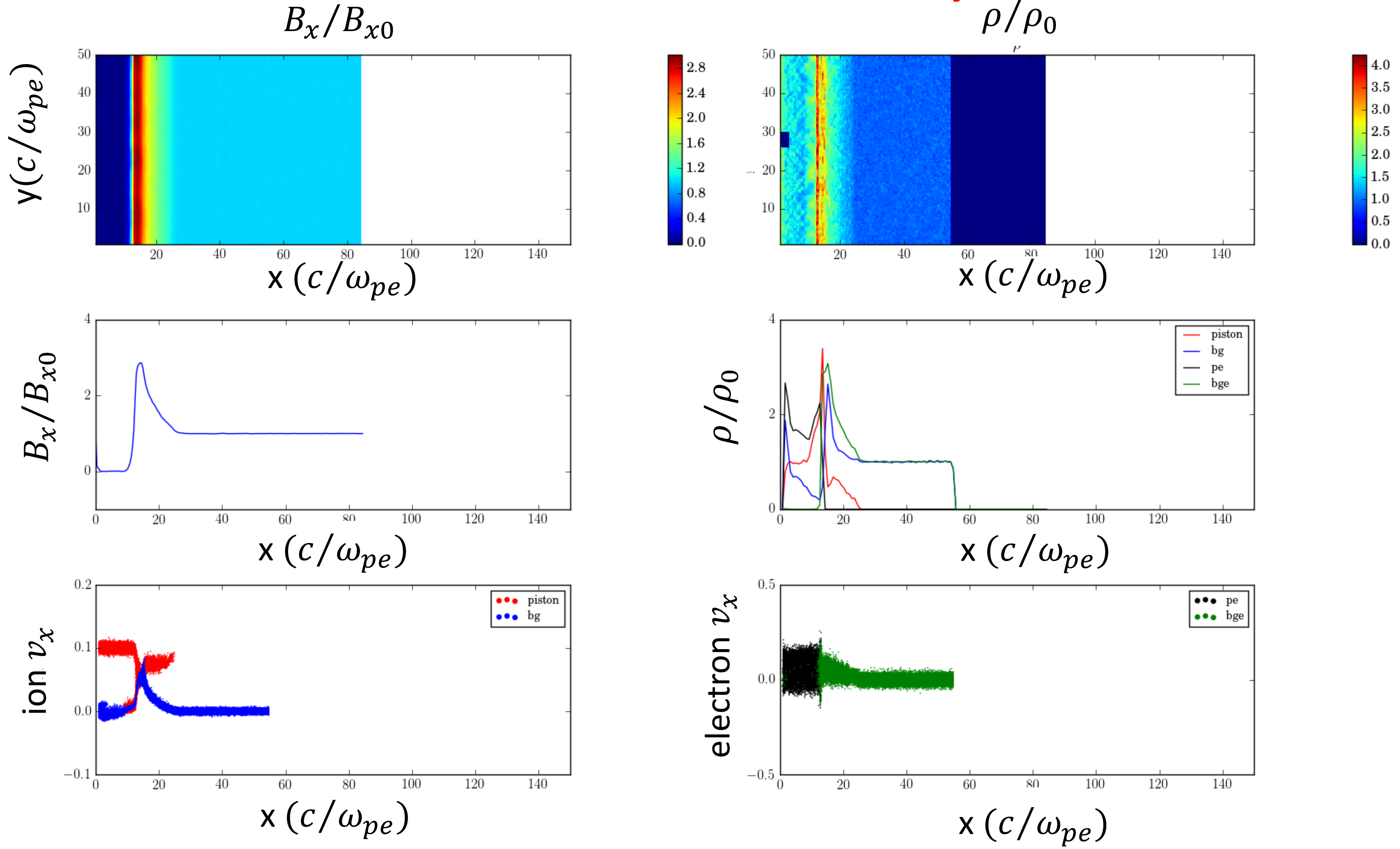

Formation of contact discontinuity: B field is compressed by piston;
background ions and electrons are reflected;
piston and background are separated.

Shock in Ion first gyration:

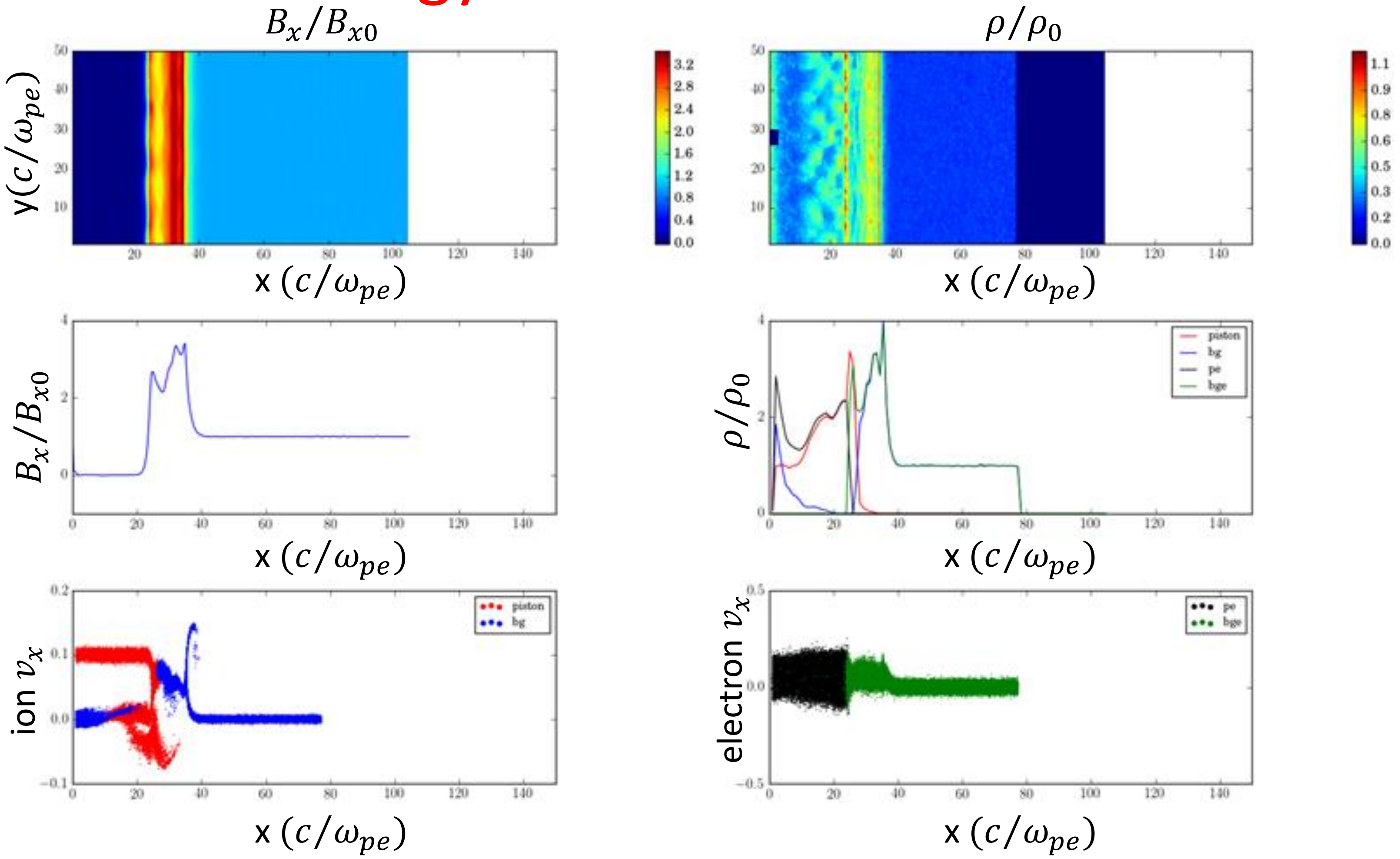

Shock in Ion first gyration: magnetic overshoot;

background ions are in the first gyration;

Fully formed shock:

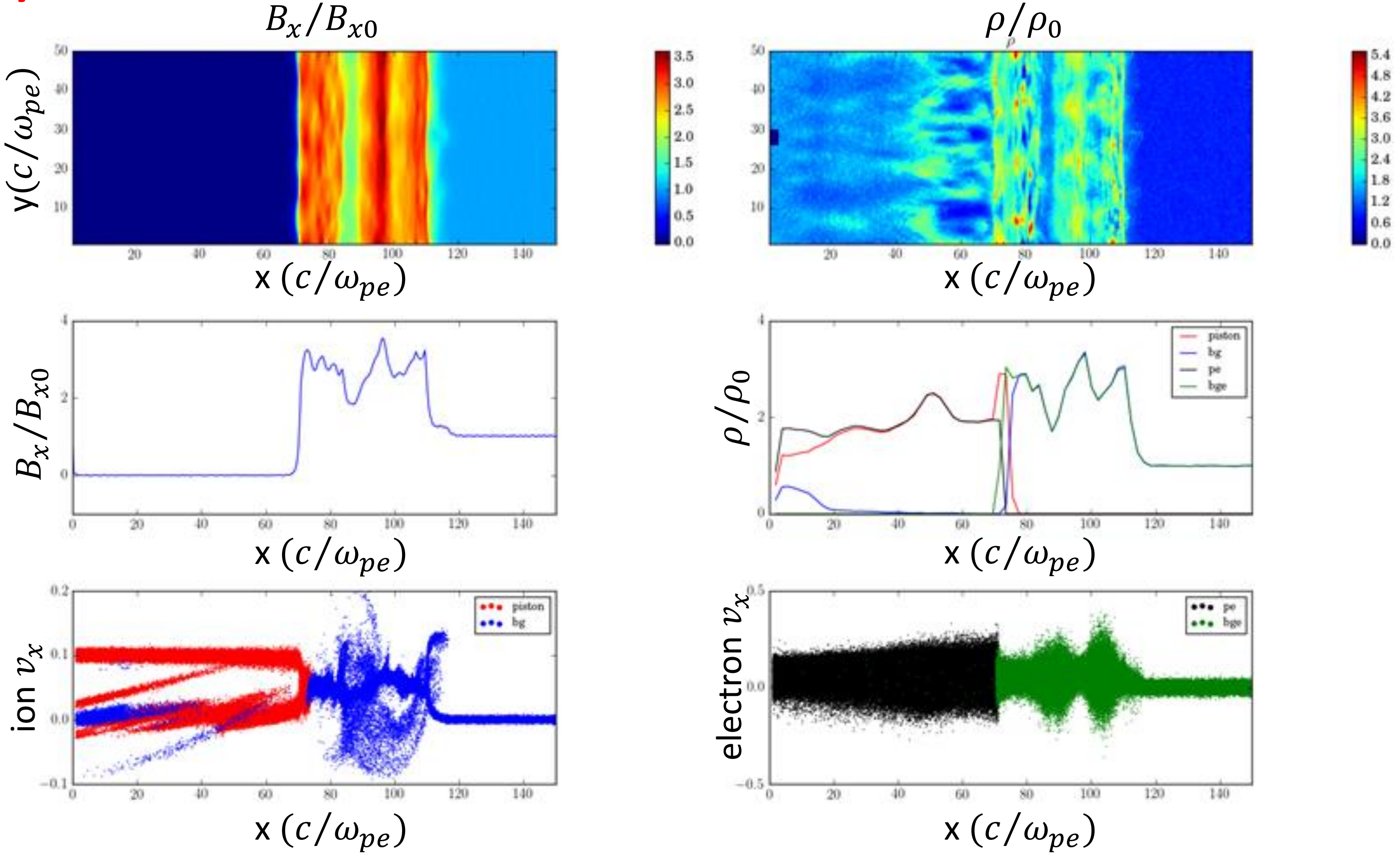

Fully formed Shock: shock becomes thicker ;

background ions show several gyrations;

Magnetized Shock Campaign on Omega-EP Laser: Principle and Target Configuration

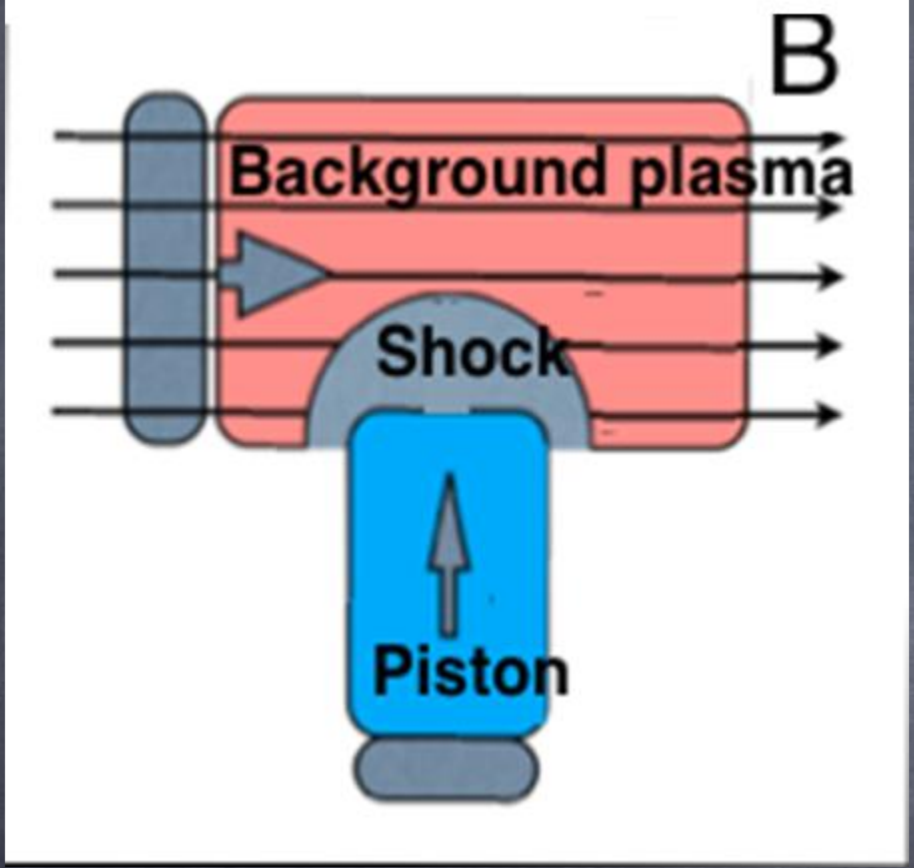

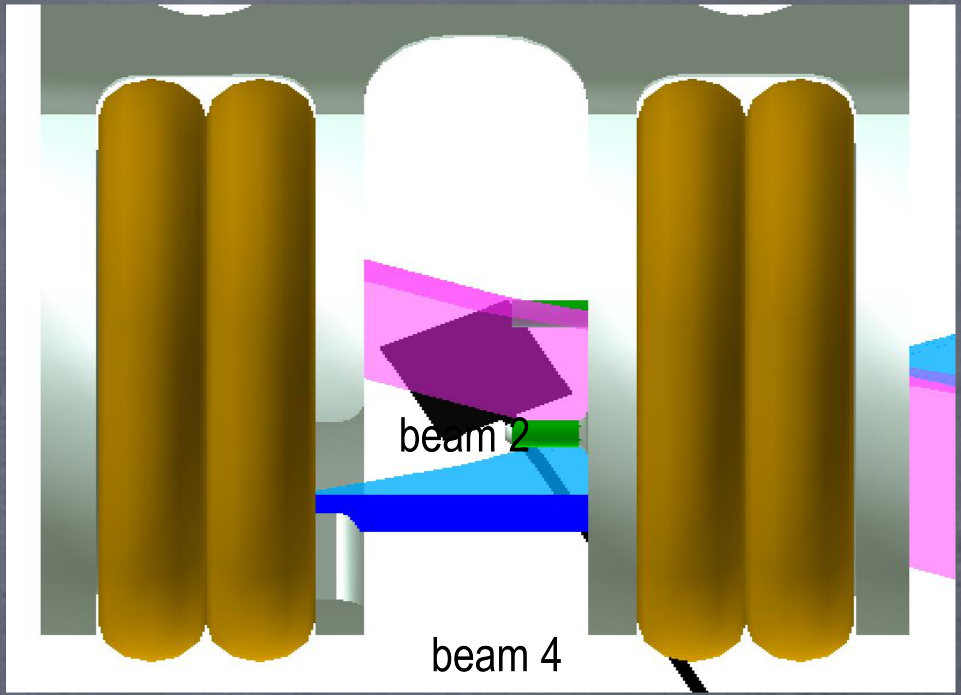

We study magnetized shock formation by driving a fast ablated piston plasma into pre-magnetized background plasma.

Piston Driven Shock Experiment on Omega-EP Laser: Diagnostic View and Proton Radiography

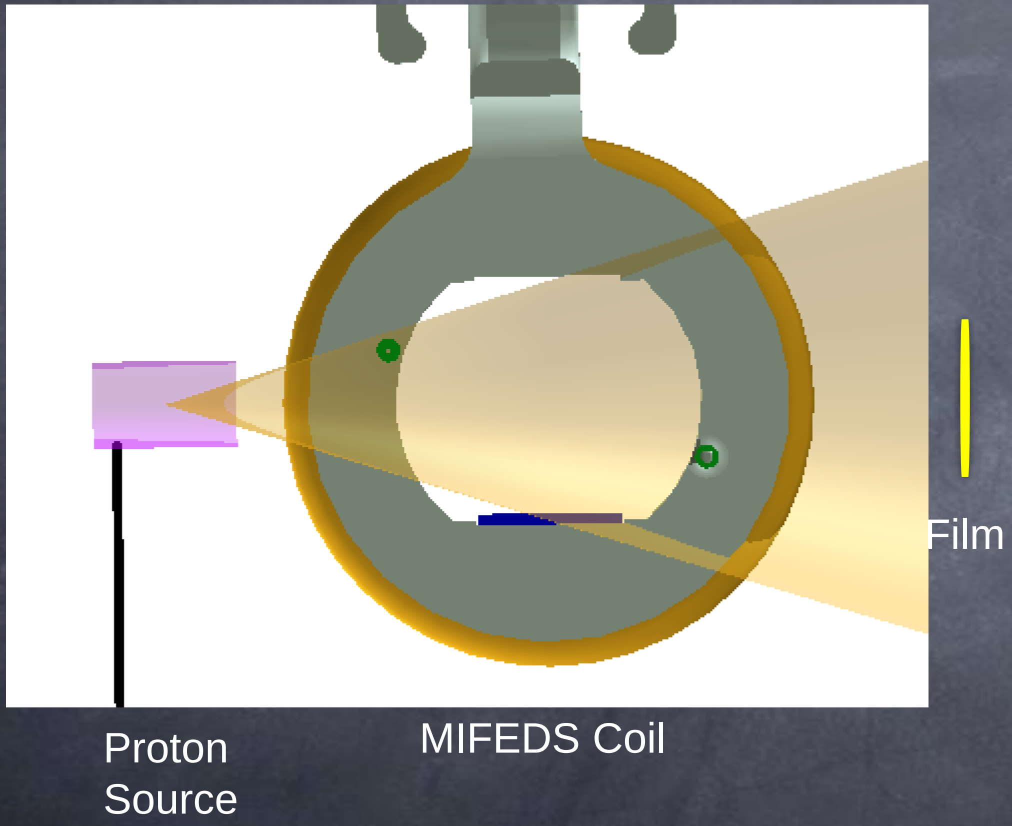

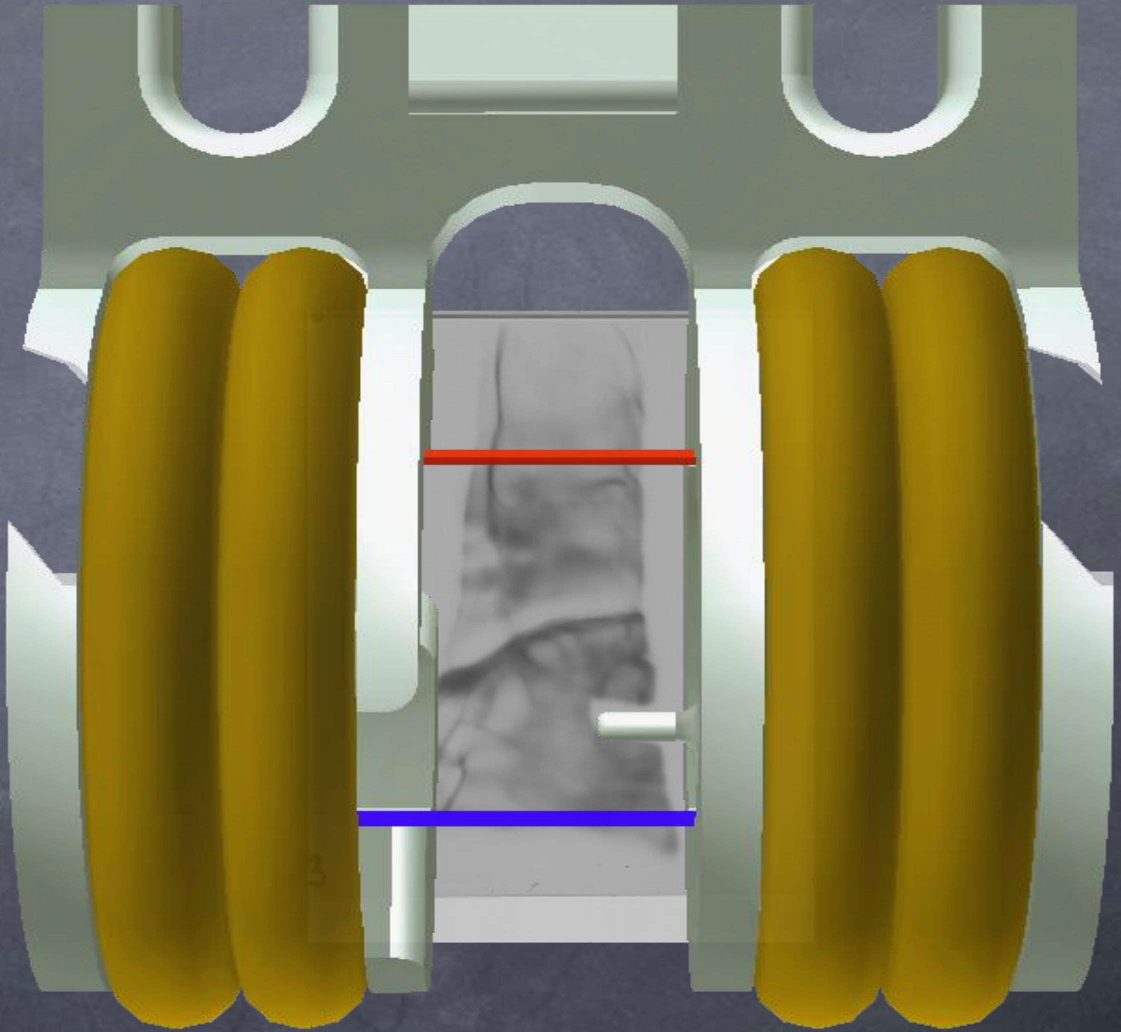

Proton radiography is main diagnostic

Proton Radiography in Experiments

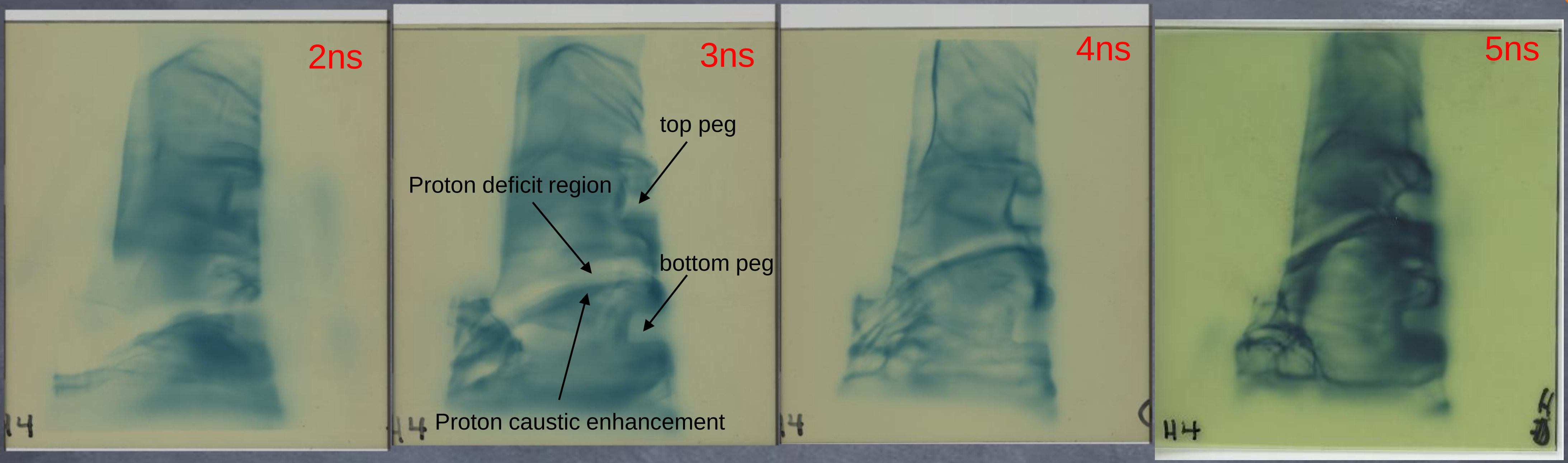

Features in radiography:

- Trapezoid Distortion
- Moving Proton deficit region followed by caustic
- Evolution of thickness of proton deficit region
- Tilted proton deficit region and caustic

Proton Radiography in Experiments

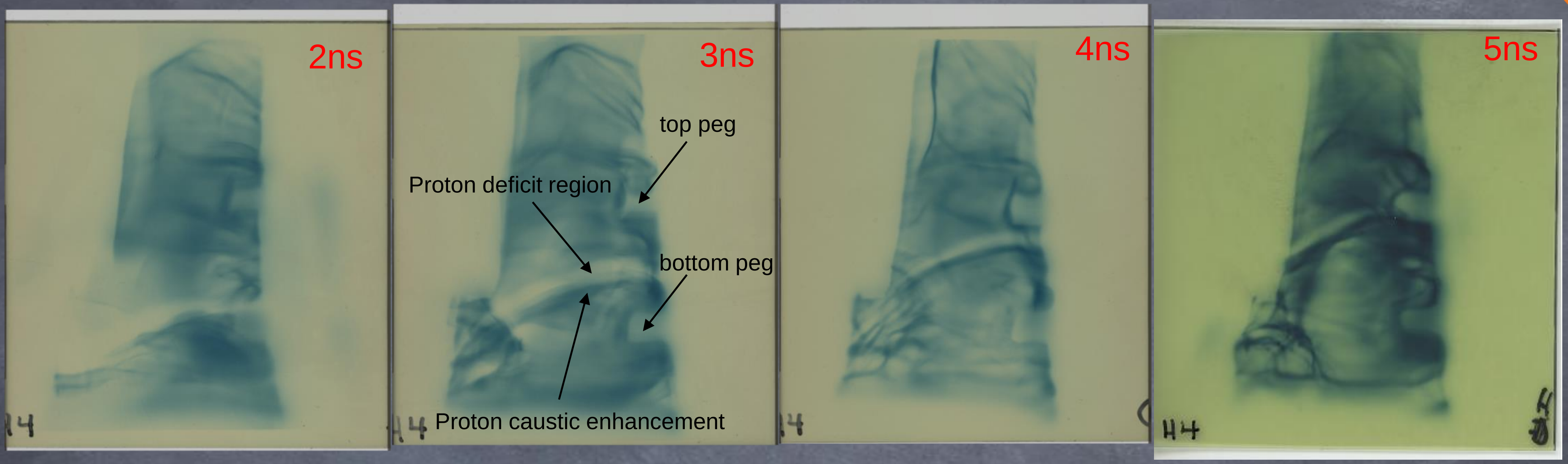

Features in radiography:

- Trapezoid Distortion
- Moving Proton deficit region followed by caustic
- Evolution of thickness of proton deficit region
- Tilted proton deficit region and caustic

Trapezoid distortion: estimation of the external B Field

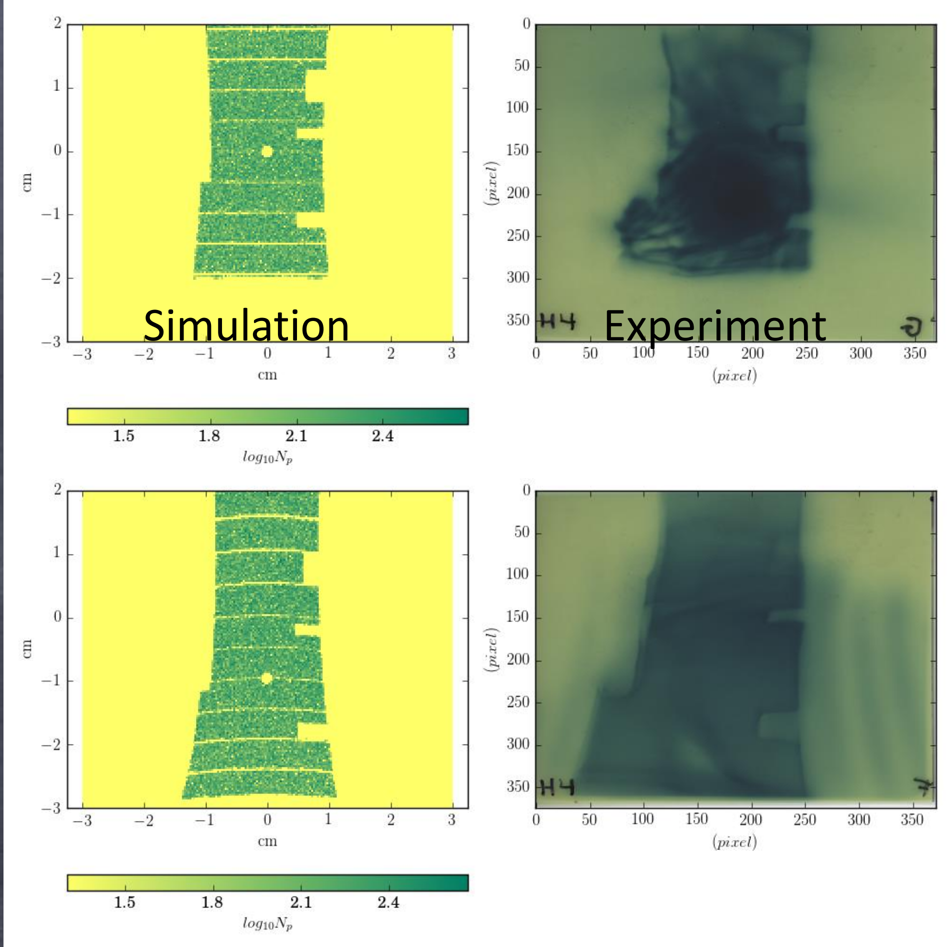

B-off: No Trapezoid Distortion

B-on: Trapezoid Distortion

Model trapezoid distortion and the distances of pegs:

External B (MIFEDS) is about 7~8T

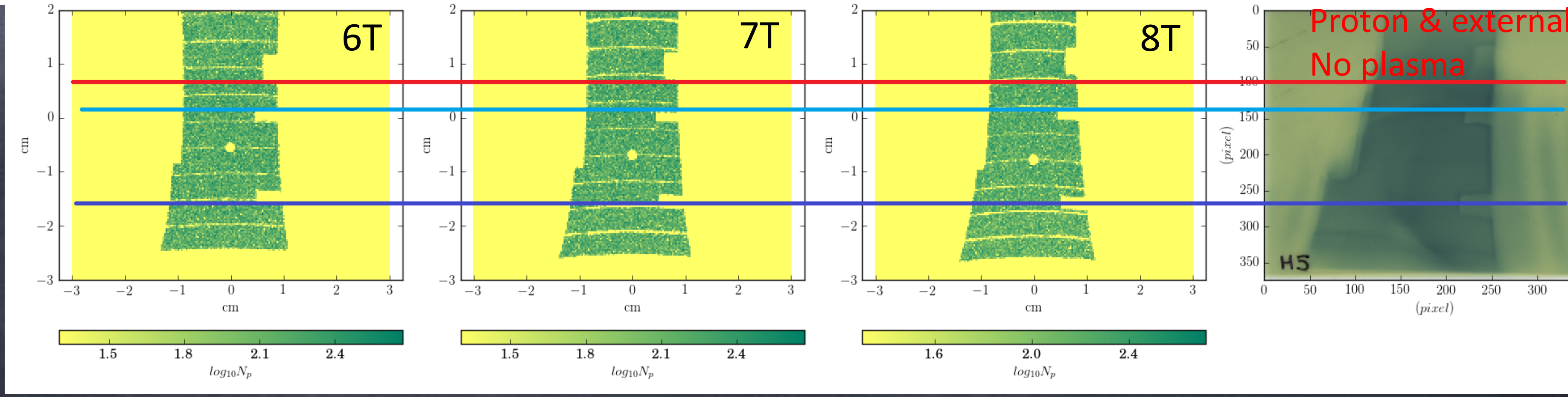

Proton Radiography in Experiments

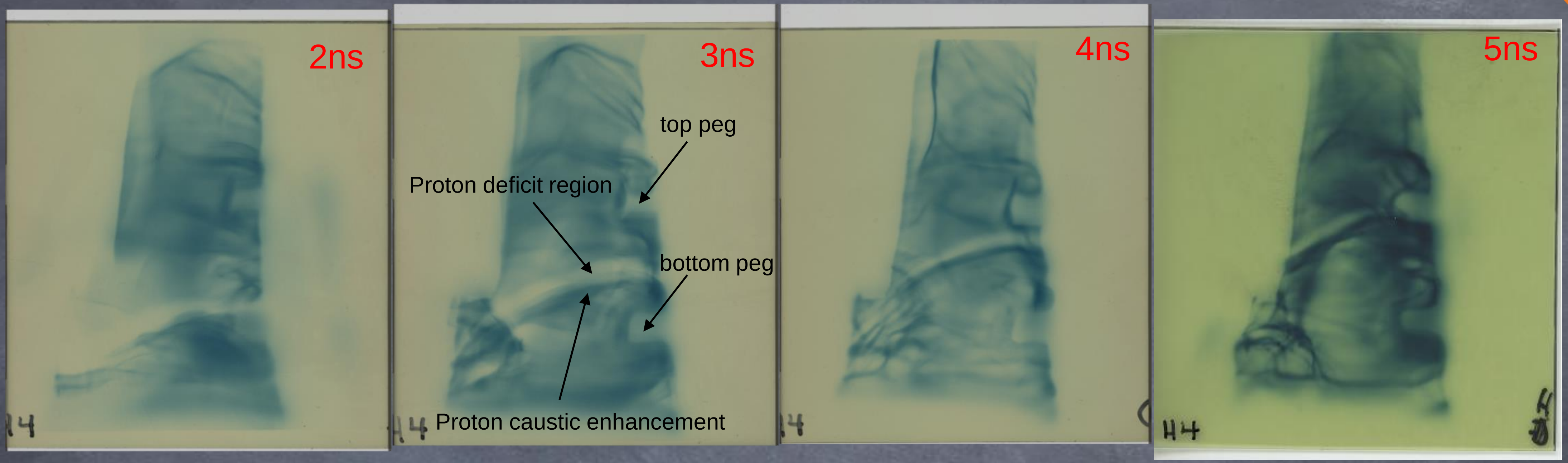

Features in radiography:

- Trapezoid Distortion
- Moving Proton deficit region followed by caustic
- Evolution of thickness of proton deficit region
- Tilted proton deficit region and caustic

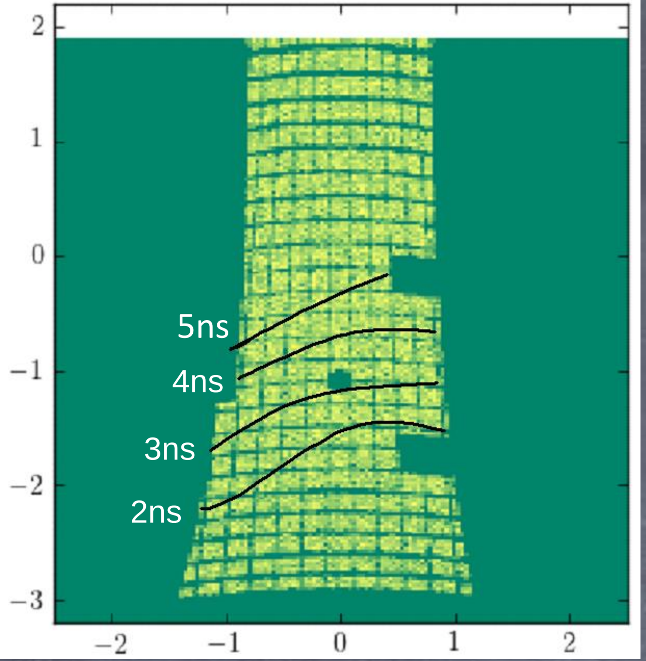

The moving feature indicates a propagating compressed B field. The feature speed is ~450 km/s, $n_e = 10^{17} - 10^{18}$ cc, $M_A = 3\sim12.$ $\lambda_{mfp} \approx 2cm >$ Diameter of Coil

Collisionless condition achieved!

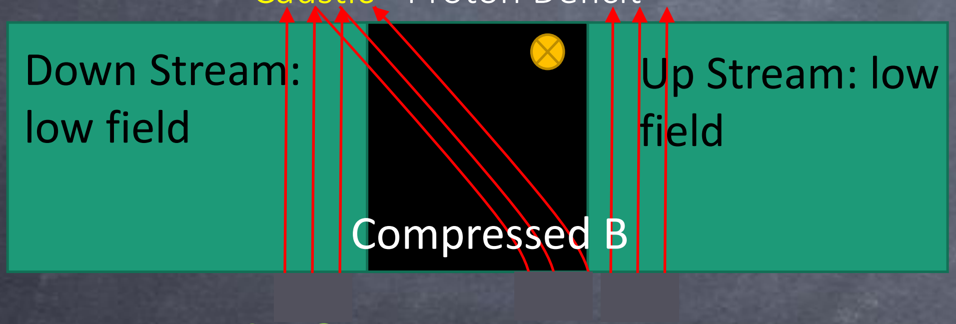

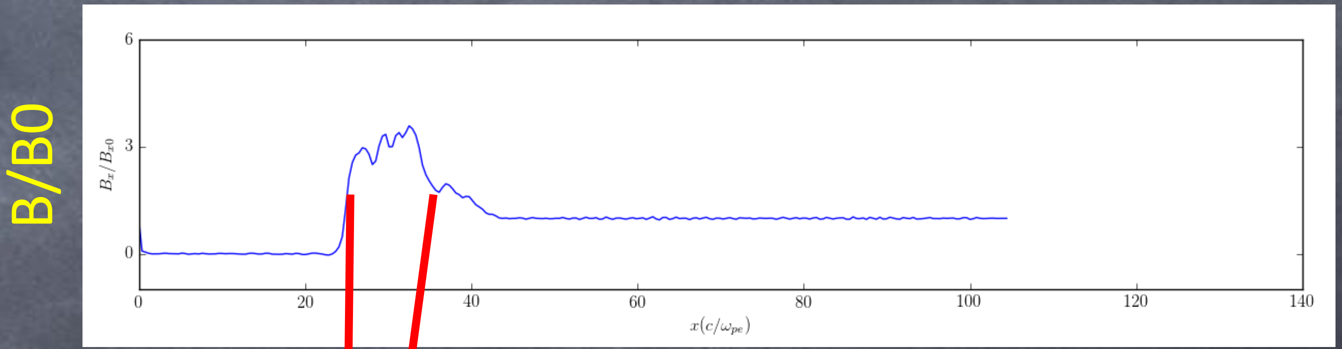

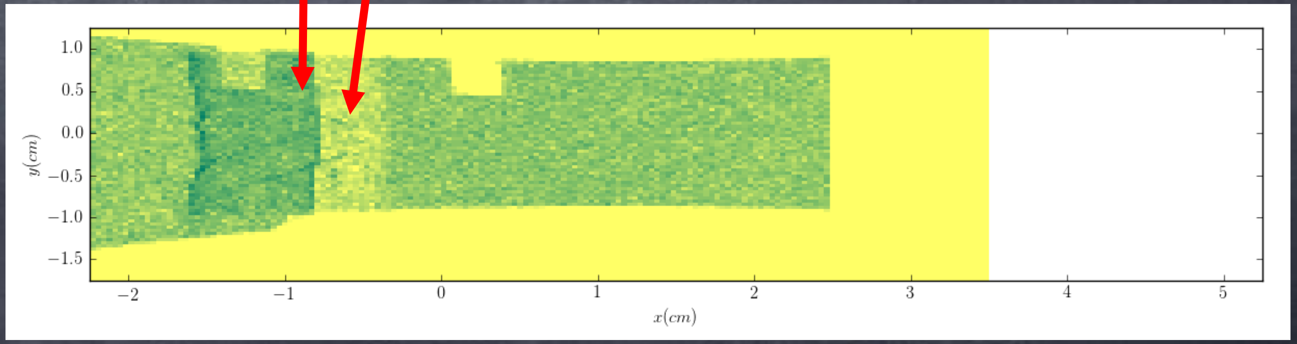

Simulated Proton Radiography

Proton deficit region:

Increasing B (from right to left)

Proton caustic enhancement:

Decreasing B

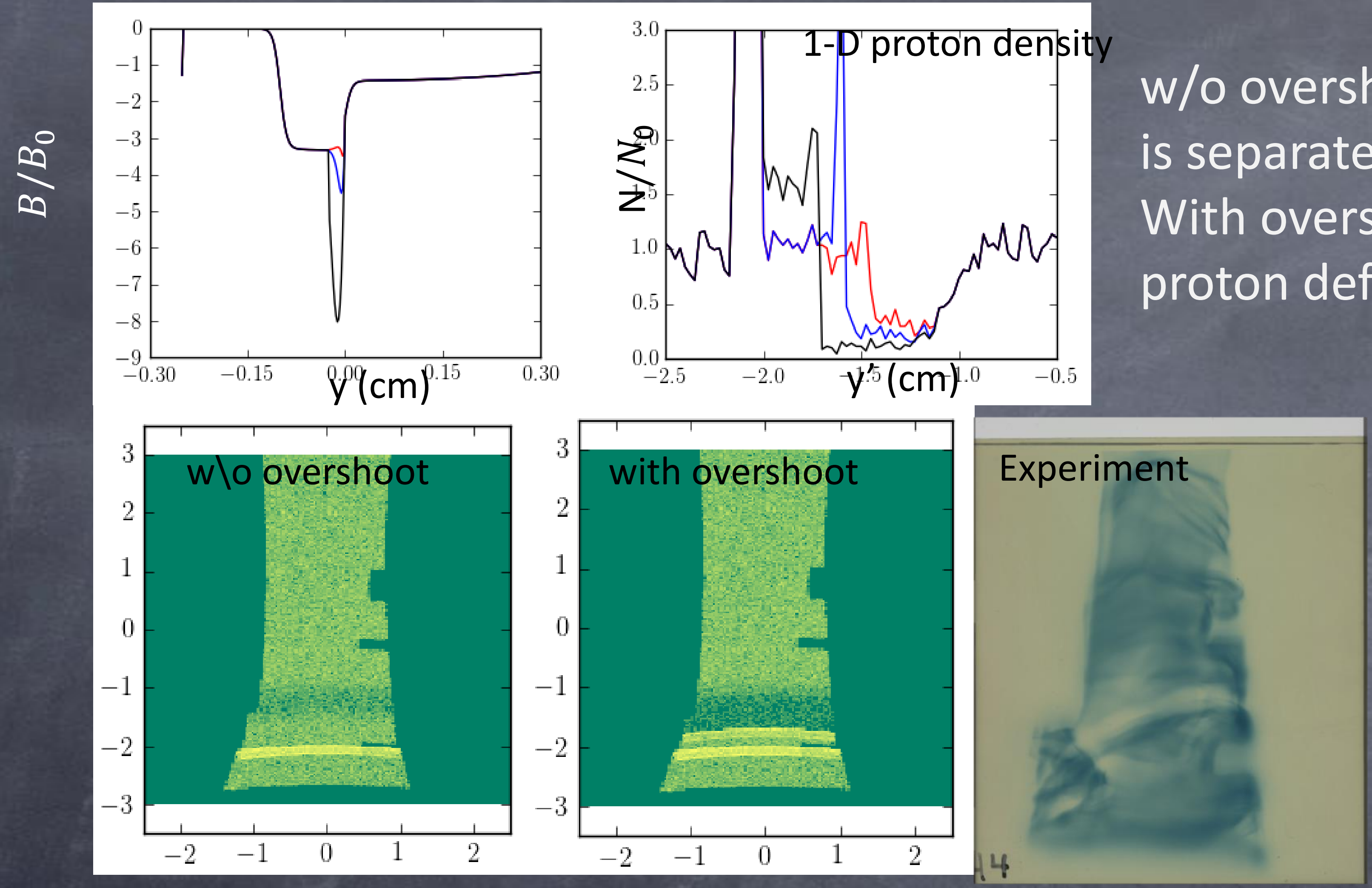

w/o overshoot the proton deficit region is separated from the caustic.
With overshoot the caustic follows the proton deficit region.

Caustic always follows proton deficit region.
Magnetic overshoot in the experiment!

Proton Radiography in Experiments

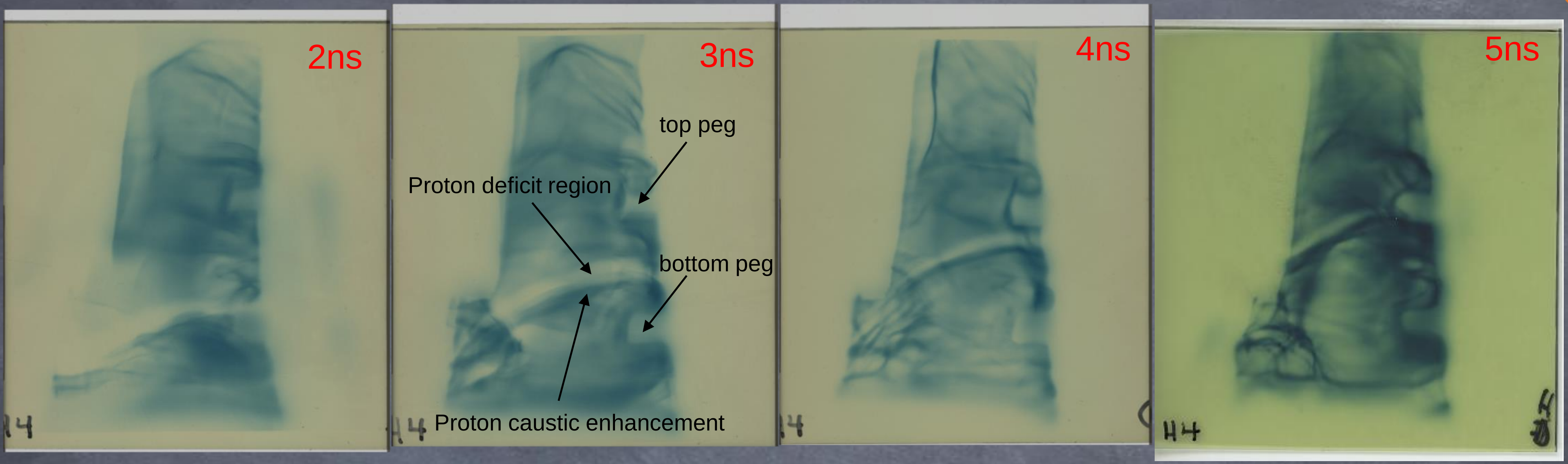

Features in radiography:

- Trapezoid Distortion
- Moving Proton deficit region followed by caustic
- Evolution of thickness of proton deficit region
- Tilted proton deficit region and caustic

Simulated Proton Radiography

$M_A = 9$, $M_S = 15$

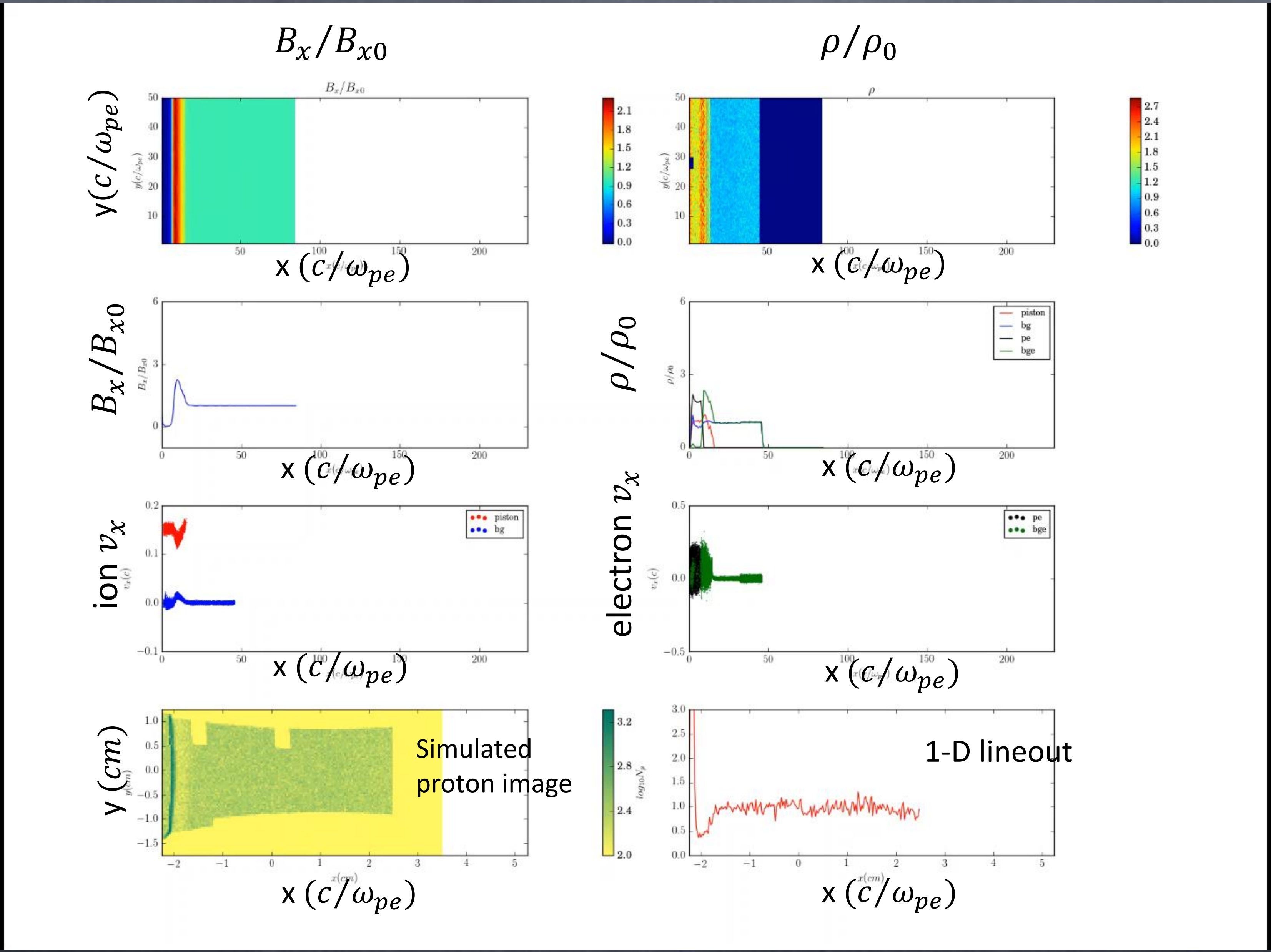

Signature of Strong Magnetized Shock: Magnetic Overshoot

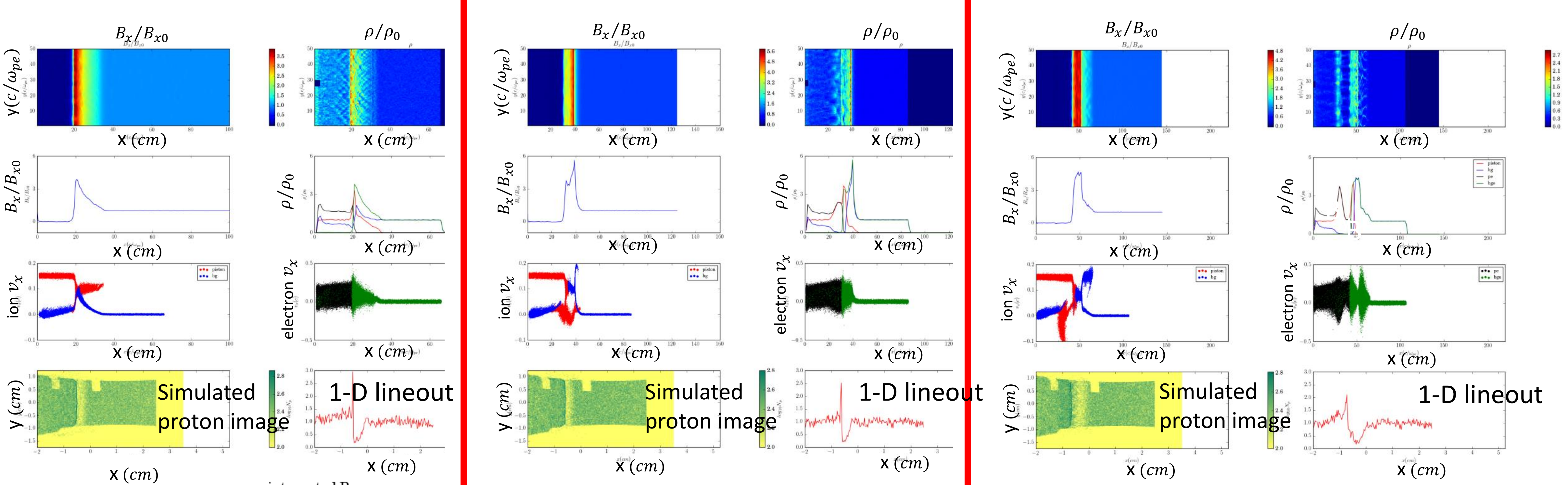

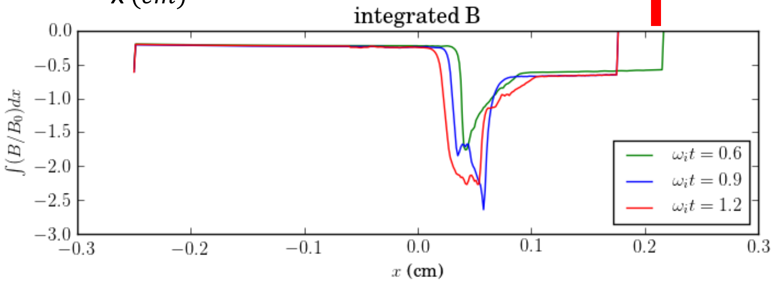

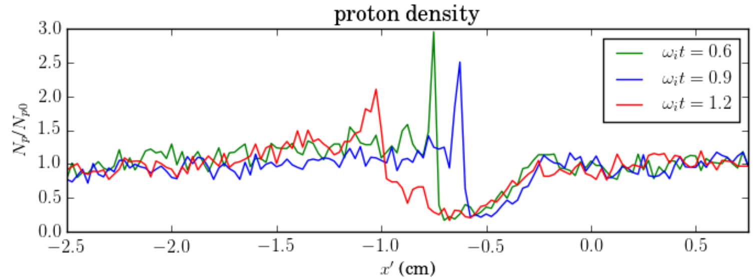

- High Mach number shocks undergo periodic reformation in the first ion loop
- Reformation leads to periodic extra magnetic compression (overshoot), proportional to M_A
- Periodic enhancement of compression leads to narrowing of proton deficit region
- *We* observe thinning of the deficit region later in time — this constrains the Mach number to be Ma > 8

M_A can be constrained with radiography only!

2-D PIC vs. Experiment

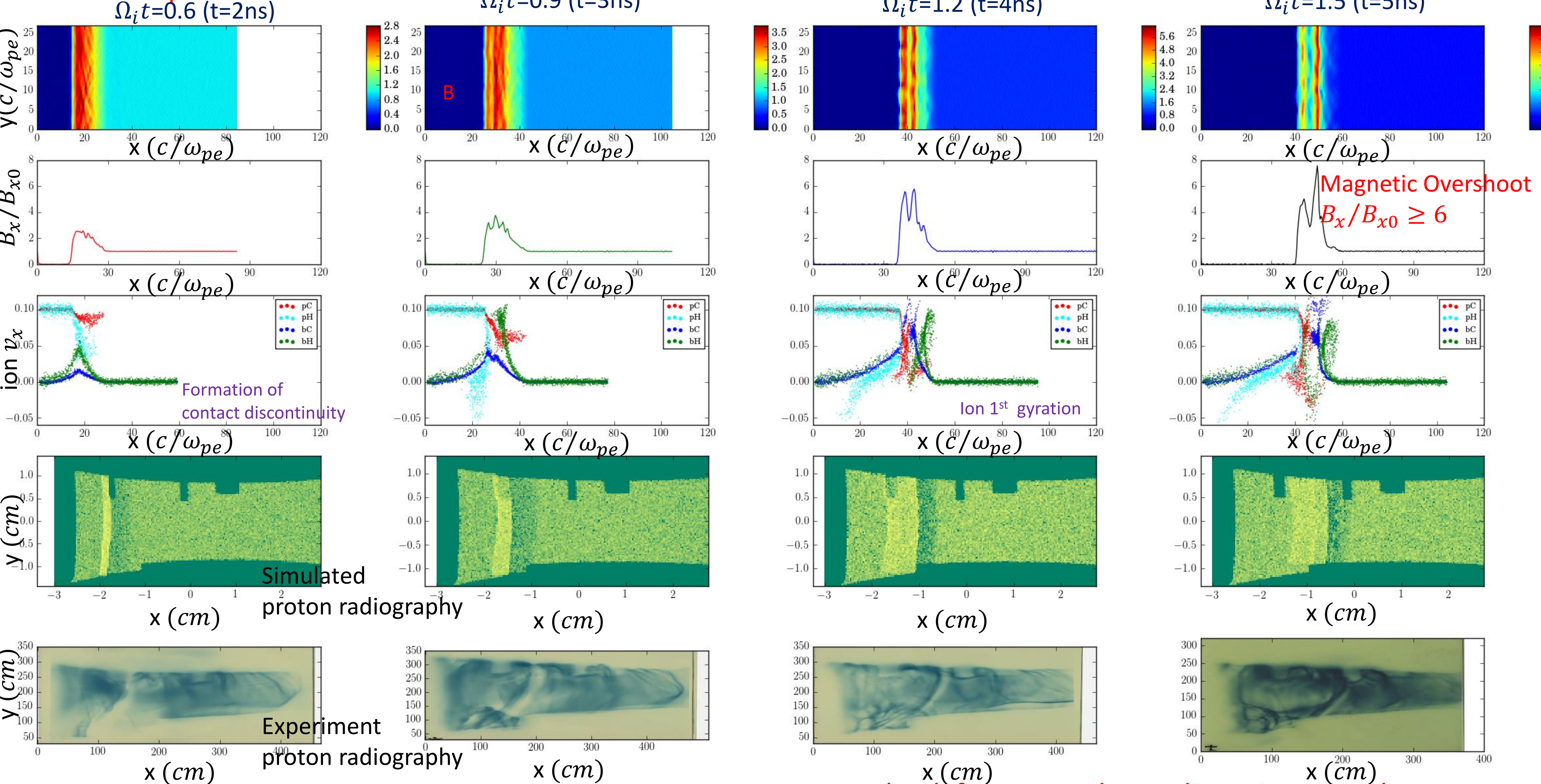

M_A = 12, M_S =10

Shock feature and speed consistent with the experiment

Proton Radiography in Experiments

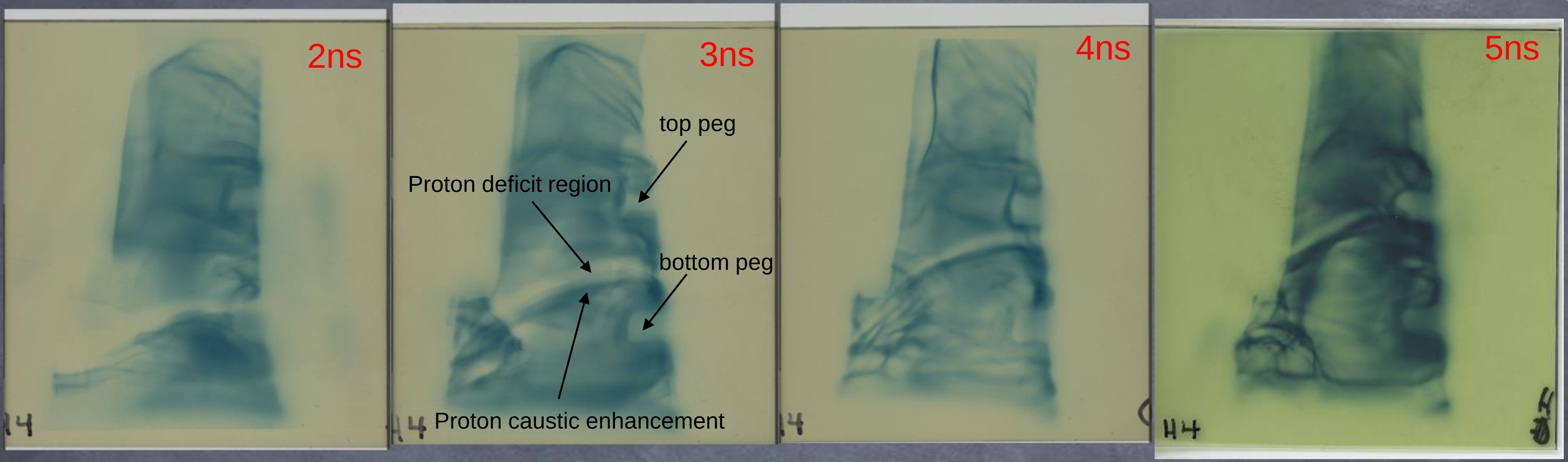

Features in radiography:

- Trapezoid Distortion
- Moving Proton deficit region followed by caustic
- Evolution of thickness of proton deficit region
- Tilted proton deficit region and caustic

3-D PIC: Experiment Configuration

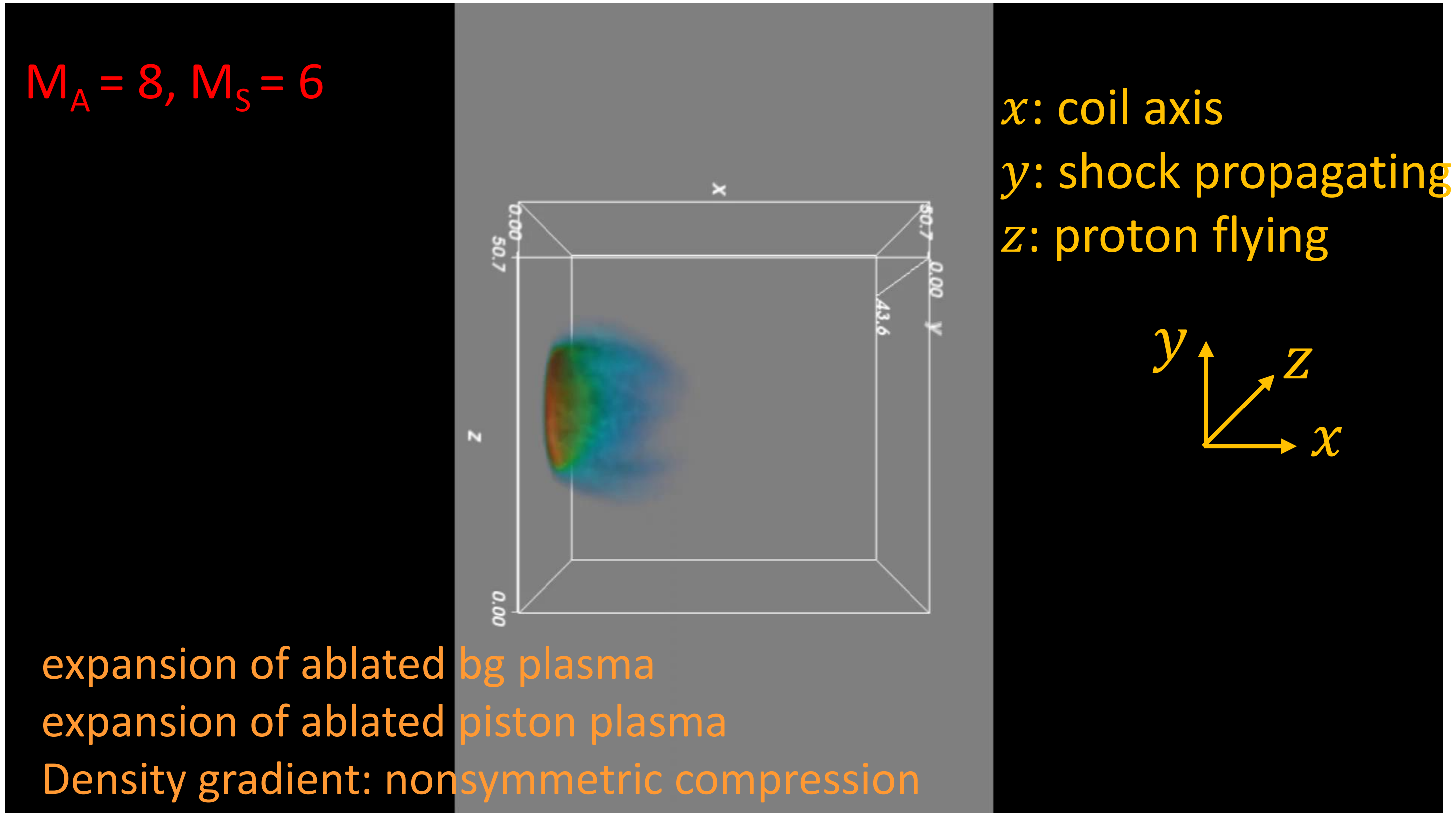

PIC vs Data: Geometry Effect

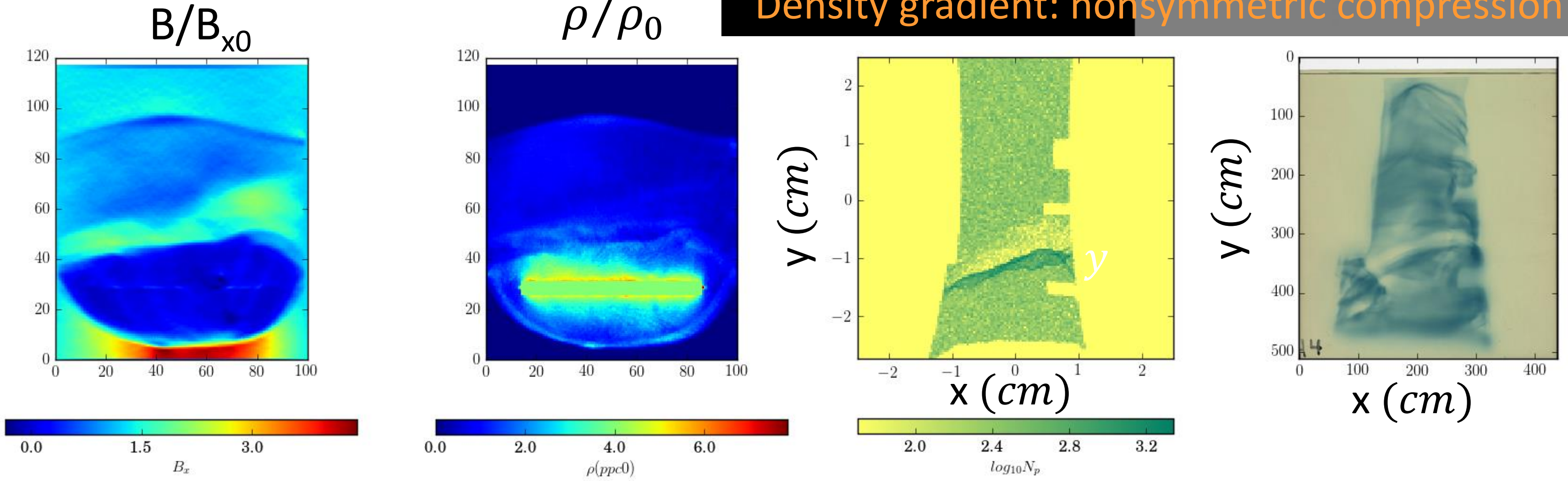

The tilted proton caustic feature is caused by density gradient of background plasma and curvature of magnetic field

Proton Radiography in Experiments

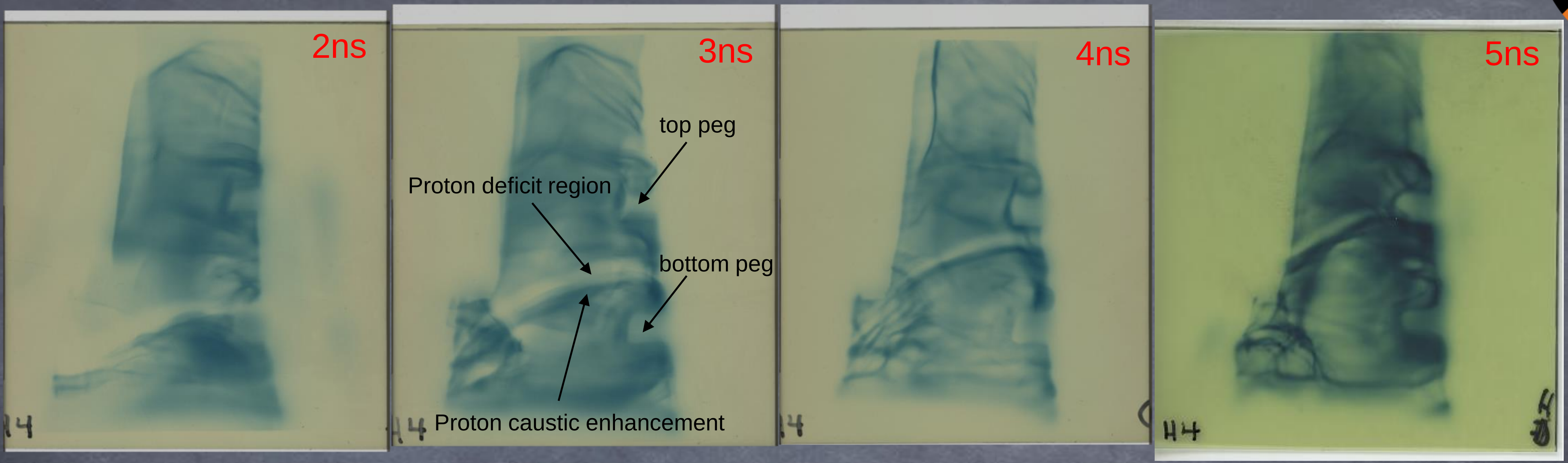

Features in radiography tell us:

- Trapezoid Distortion: External B field is 7~8 T.
- Moving Proton deficit region followed by caustic:
  Compressed magnetic field with magnetic overshoot
- Evolution of thickness of proton deficit region:
  A strong magnetic overshoot
- Tilted proton deficit region:
  Background density gradient and B-field curvature

The formation of a high Mach number magnetized shock!

Conclusion:

The experiment generates a piston-driven collisionless shock in a magnetized background plasma.

The proton radiography shows a moving compressed magnetic field with speed of 450km/s.

The proton-deficit-region narrowing indicates a strong magnetic overshoot and constrains the $M_A > 8$.

The 3-D PIC simulations explain well the tilted proton-deficit and caustic feature.

The experiment achieved the formation of a high Mach number ($M_A \approx 8 - 12$) magnetized collisionless shock.

3-D Gyrokinetic Electron and Fully Kinetic Ion (GeFi) Particle Simulation of Current Sheet Instabilities

Motivation: Magnetic Reconnection

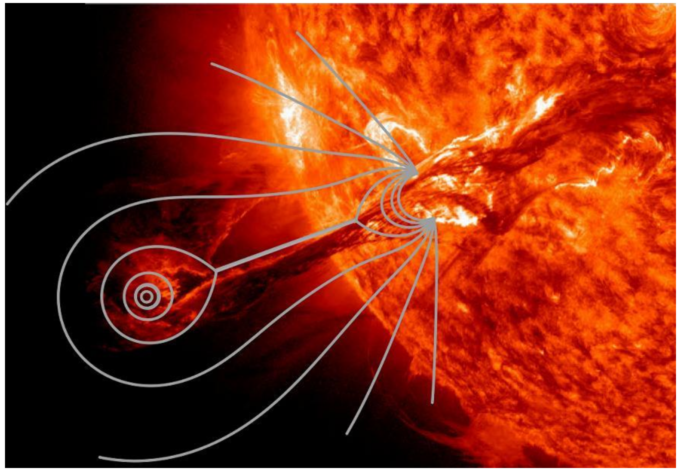

A CME event in the solar atmosphere (SDO, NASA)

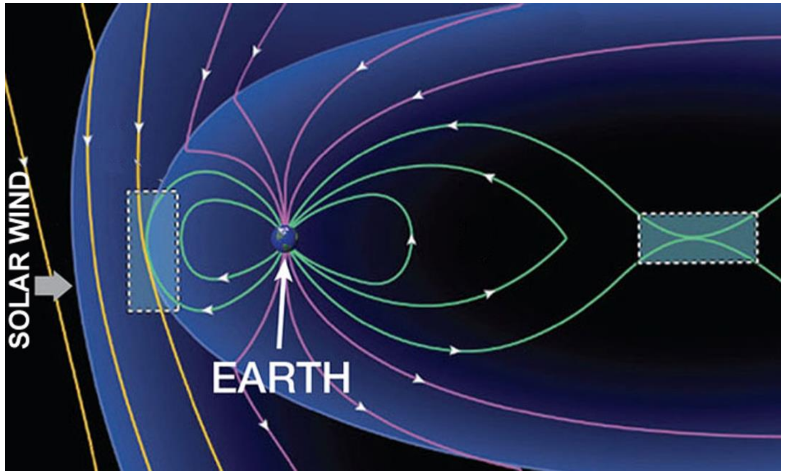

Reconnection in magnetosphere (MMS, NASA)

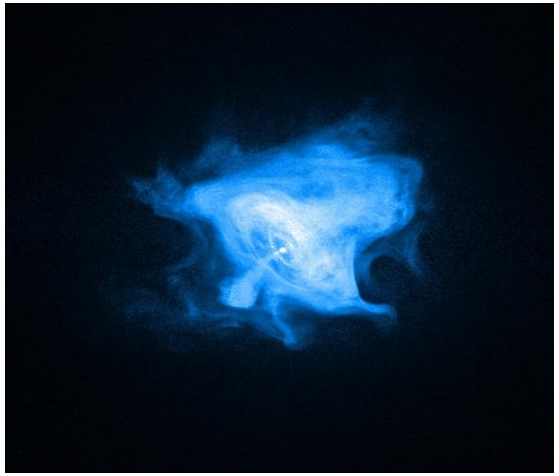

Pulsar wind Nebulae (NASA)

Laboratory experiment in MRX

Current Sheet Instabilities

- Current sheet instabilities mediate the onset of magnetic reconnection, e.g., plasmoids formation, turbulence, and current sheet disruption.
- The current sheet instabilities in lower-hybrid frequency range are thought to introduce the turbulences[Che 2017, Muñoz and Büchner 2018]. Observations and experiments found lower-hybrid frequency waves in reconnection region [Zhou *et al.* 2009, Carter *et al.* 2001, Ji *et al.* 2004, Khotyaintsey *et al.* 2016, Ergun *et al.* 2016, Zhou *et al.* 2016, Wilder *et al.* 2016]. 3-D PIC simulations showed the fluctuations and turbulences in the lower-hybrid frequency range [Le *et al.* 2018, Muñoz and Büchner 2018]. The studies motivate us to survey the current sheet instabilities.
- Lower-hybrid-drift instability [Daughton 2003] and Buneman instability [Yoon and Lui 2008] had been found in lower-hybrid frequency range. In this study, we use gyrokinetic electron and fully kinetic ion (GeFi) particle simulation code to systematically survey the current sheet instabilities under a broad range of guide magnetic field with the realistic ion-to-electron mass ratio.

The Necessity of Developing Gyrokinetic Electron and Fully kinetic Ion Particle Scheme

- In both space and laboratory plasmas:

  Reconnection involves a wide range of spatial and temporal scales.
  low-frequency MHD $\longrightarrow$ lower-hybrid/whistler
  electron Larmor radius $\longrightarrow$ system size

- Fully kinetic explicit PIC simulations have been used to study reconnection and made significant progresses, but often with a reduced ion-to-electron mass ratio to accommodate available computing resources.

  Fully kinetic explicit PIC models resolve high frequency gyromotion of electrons and thus need a timestep smaller than electron gyrofrequency.

In many low-frequency ($\omega < \Omega_e$) problems, resolving electron cyclotron motion is not necessary.

In the GeFi Model [*Lin et al*., 2005, 2011]

- Electrons are treated as gyrokinetic (GK) particles, and ions are treated as fully kinetic particles.
- The rapid electron cyclotron motion is removed while finite Larmor radius effects are retained.
- Because electrons and ions are on the equal footing, the GeFi scheme allows a larger time step ($\sim\Omega_e$) and can handle a realistic ion-to-electron mass ratio.
- Speed up: in some test cases, GeFi can be 20~50 times faster than the fully kinetic explicit δf particle simulation scheme.

- **This work**: Use GeFi particle code [*Lin et al*., 2005, 2011] to investigate current sheet instabilities with:
  a wide range of B_G*;*
  realistic mass ratio m_i/m_e*;*
  full 3-D space.

- To validate GeFi scheme and code, the GeFi results are **compared with** the *fully kinetic* δf *particle simulations* and GK *analytic eigen theory* [*Tummel et al*., 2014].

2. GeFi Simulation Scheme

Gyrokinetic formulation requires system must obey the GK ordering,

$$\frac{\omega}{\Omega_e} \sim \frac{\rho_e}{L} \sim k_\parallel \rho_e \sim \frac{\delta B}{B} \sim \epsilon,$$

$$k_\perp \rho_e \sim 1.$$

where L is the macroscopic background plasma scale length, δB is the perturbed magnetic field on the microscopic wave scale lengths, and ε is a smallness parameter.

2.1 Particle advance

Fully kinetic ions in 6-D phase space (**x**, **v**):

$$\frac{\partial f_\mathrm{i}}{\partial t} + \dot{x}_\mathrm{i} \cdot \frac{\partial f_\mathrm{i}}{\partial x_\mathrm{i}} + \dot{p}_\mathrm{i} \cdot \frac{\partial f_\mathrm{i}}{\partial p_\mathrm{i}} = 0, \quad (1)$$

Adopting the PIC scheme, the evolution of f_i is determined by ion equation of motion:

$$\frac{\mathrm{d}}{\mathrm{d}t} p_\mathrm{i} = -q_\mathrm{i} \nabla(\phi - v_\mathrm{i} \cdot \boldsymbol{A}/c), \quad (2)$$

$$\frac{\mathrm{d}}{\mathrm{d}t} x_\mathrm{i} = v_\mathrm{i} = (p_\mathrm{i} - q_\mathrm{i} \boldsymbol{A}/c)/m_\mathrm{i}, \quad (3)$$

The number density and current density are obtained from the velocity moments of f_i:

$$n_\mathrm{i} = \int f_\mathrm{i}\, \mathrm{d}^3 v = \sum_j \delta(\boldsymbol{x} - \boldsymbol{x}_j), \quad (4)$$

$$\boldsymbol{J}_\mathrm{i} = q_\mathrm{i} \int v f_\mathrm{i}\, \mathrm{d}^3 v = q_\mathrm{i} \sum_j v_j \delta(\boldsymbol{x} - \boldsymbol{x}_j) \quad (5)$$

Gyrokinetic electrons in 5-dimensional space $(\vec{R}, v_{\|}, \mu)$:

GK equations of motion [*Frieman and Chen*, 1982; *Hahm, Lee, and Brizard*, 1988; *Brizard*, 1989]:

$$\frac{\mathrm{d}p_{\|}}{\mathrm{d}t} = -\boldsymbol{b}^* \cdot [q_e \langle \nabla \phi^* \rangle + \mu \nabla \bar{B}], \qquad (6)$$

$$\frac{\mathrm{d}\boldsymbol{R}}{\mathrm{d}t} = v_{e\|}\boldsymbol{b}^* + \frac{c}{q_e \bar{B}} \bar{\boldsymbol{b}} \times [q_e \langle \nabla \phi^* \rangle + \mu \nabla \bar{B}], \qquad (7)$$

$p_{\|}=m_e v_{e\|}+q_e A_{\|}/c$, **R** is the gyrocenter position, μ is the magnetic moment, $\mathbf{b}^*=\mathbf{b}+(v_{e\|}/\Omega_e)\mathbf{b}\times(\mathbf{b}\bullet\nabla)\mathbf{b}$, b=**B**/B, **b**=**B**/B, **B**=**B**+ δ**B**, **B** is the averaged magnetic field, $\delta\mathbf{B}=\nabla\times\mathbf{A}$, $\phi^*=\phi-\mathbf{v}\bullet\mathbf{A}/c$, ϕ and A are scalar and vector potentials, and <…> means gyro-averaging.

2.2. Field Calculation:

to solve vector and scalar potential **A** and ϕ, we need to obtain electron moments in particle-phase space.

Under nonlinear GK formulism, the electron distribution function can be written as

$$f = \bar{f} + \frac{q\phi}{m}\frac{\partial \bar{f}}{\partial w} + T_{\mathrm{g}}^{-1}(\delta G), \tag{9}$$

where $\bar{f}$ is the background distribution function in the gyrocenter coordinates and $T_g^{-1} = \exp(\rho \cdot \nabla_{\perp})$ is the pull-back operator from gyrocenter coordinates to guiding-center coordinates.

Eq. (9) can be further written as

$$f = \frac{q}{m}\frac{\partial \bar{f}}{\partial w}\left[\phi - T_{\mathrm{g}}^{-1}\left\langle T_{\mathrm{g}}\left(\phi - \frac{1}{c}v \cdot A_{\perp}\right)\right\rangle\right] + T_{\mathrm{g}}^{-1}F. \tag{10}$$

Substituting (10) into $n_e = \int f d^3 v$, the electron density n_e can be expressed as

$$n_{\mathrm{e}} = \frac{q_{\mathrm{e}}}{m_{\mathrm{e}}}\int \mathrm{d}^3 v \left(\frac{\partial \bar{f}_{\mathrm{e}}}{\partial w}\right)\left[\phi - \langle\phi\rangle + \frac{1}{c}\langle v_{\perp} \cdot A\rangle\right] + \langle N_{\mathrm{e}}\rangle. \tag{11}$$

Substituting (11) into Poisson's equation, assuming $|\nabla_\perp^2| >> |\nabla_\|^2|$, generalized GK Poisson's equation:

$$\left(1+\frac{\bar{\omega}_{\mathrm{pe}}^2}{\bar{\Omega}_{\mathrm{e}}^2}\right)\nabla_\perp^2\phi + 4\pi\bar{n}_{\mathrm{e}}q_{\mathrm{e}}\frac{\delta B_\|}{\bar{B}} = -4\pi\left(q_{\mathrm{i}}n_{\mathrm{i}} + q_{\mathrm{e}}\langle N_{\mathrm{e}}\rangle\right), \qquad (12)$$

where $\bar{n}_e$ is the spatially averaged n_e, $\langle N_e \rangle$ is electron gyro-averaged guiding center density.

Note that, for the first time, the fast-mode compressional/whistler waves are included in the Poisson's equation of a GK particle model by $\delta B_\|$ term.

To calculate $\delta B_{\parallel}$, the electron force balance equation

$$\nabla \cdot (n_e q_e \boldsymbol{E}) = \nabla \cdot \left[\nabla \cdot \boldsymbol{P}_e - \frac{1}{c} \boldsymbol{J}_e \times \boldsymbol{B} \right], \tag{13}$$

is used, where

$$\boldsymbol{P}_e = \left(\bar{n}_e q_e \rho_e^2 \nabla_\perp^2 \phi + 2 \bar{n}_e T_e \frac{\delta \bar{B}_\parallel}{\bar{B}} \right) \left(\boldsymbol{I} - \frac{1}{2} \bar{\boldsymbol{b}} \bar{\boldsymbol{b}} \right) + \langle \boldsymbol{P}_g \rangle,$$

$$\langle \boldsymbol{P}_g \rangle = \int m_e \boldsymbol{v} \boldsymbol{v} F_e \, \mathrm{d}^3 v, \qquad \text{(gyro-averaged guiding center moment)}$$

Define a scalar function Ψ as

$$\Psi = \frac{(1 + \bar{\beta}_e) \bar{B} \delta B_\parallel}{4\pi} - \bar{n}_i q_i (1 + \rho_e^2 \nabla_\perp^2) \phi. \tag{14}$$

The force balance equation can be expressed as

$$\nabla^2 \Psi = -\nabla \cdot \left(\nabla \cdot \boldsymbol{P}_g + \frac{1}{c} \boldsymbol{J}_i \times \boldsymbol{B} \right) \tag{15}$$

Expressing $\delta B_{||}$ in terms of ψ, the GK Poisson's equation finally is

$$\left[\left(1+\bar{\beta}_{\mathrm{e}}+\frac{\bar{\omega}_{\mathrm{pe}}^{2}}{\bar{\Omega}_{\mathrm{e}}^{2}}\right)\nabla_{\perp}^{2}-\frac{\bar{\omega}_{\mathrm{pi}}^{2}}{\bar{V}_{A}^{2}}\right]\phi=-4\pi\left[(1+\bar{\beta}_{\mathrm{e}})(q_{\mathrm{i}}n_{\mathrm{i}}+q_{\mathrm{e}}\langle N_{\mathrm{e}}\rangle)-\frac{4\pi\bar{n}_{\mathrm{i}}q_{\mathrm{i}}}{\bar{B}^{2}}\Psi\right], \qquad (16)$$

Where $\bar{\omega}_{pi}$ and $\bar{V}_A$ are the background ion plasma frequency and the Alfven speed.

We solve equations (15) and (16) by iterations to completely determine ϕ, and $\delta B_{||}$.

Then calculating $\boldsymbol{A}$, decompose $\boldsymbol{A}$ as $\boldsymbol{A} = \boldsymbol{A}_{\perp} + A_{\|}\hat{\boldsymbol{b}} + \nabla_{\perp}\xi$. The Coulomb gauge is used.

$\boldsymbol{A}_{\perp}$ is determined by the perpendicular Ampere's law,

$$\nabla^{2}\boldsymbol{A}_{\perp}=-\frac{4\pi}{c}\boldsymbol{J}_{\perp}, \qquad (17)$$

with $\boldsymbol{J}_{\perp} = (c/4\pi)\nabla \times \delta B_{\|}$.

The $A_{\|}$ is given by the following ***parallel Ampere's law***:

$$\left(\nabla^2 - \frac{\omega_{\mathrm{pe}}^2}{c^2}\right) A_{\|} = -\frac{4\pi}{c}\left(J_{\mathrm{i}\|} + \langle J_{e\|}\rangle\right). \tag{18}$$

$\langle J_{e\|}\rangle$ is the electron gyro-averaged guiding center $p_{\|}$-current.

Finally, $\nabla_{\perp}\xi$ is determined by the Coulomb gauge,

$$\nabla_{\perp}^2 \xi = -\nabla \cdot (A_{\|}\bar{b}) \tag{19}$$

Equations (17) and (18) completely determine A.
Eq. (19) ensures the Coulomb gauge.

In this study, we calculate the current sheet instabilities by using the ***linearized δf*** *and* ***nonlinear δf*** scheme.

2.4 Benchmark of GeFi code

Comparison of GeFi results with

Fully kinetic (FK) theory results and FK particle simulation results

1. GeFi results vs. FK theory

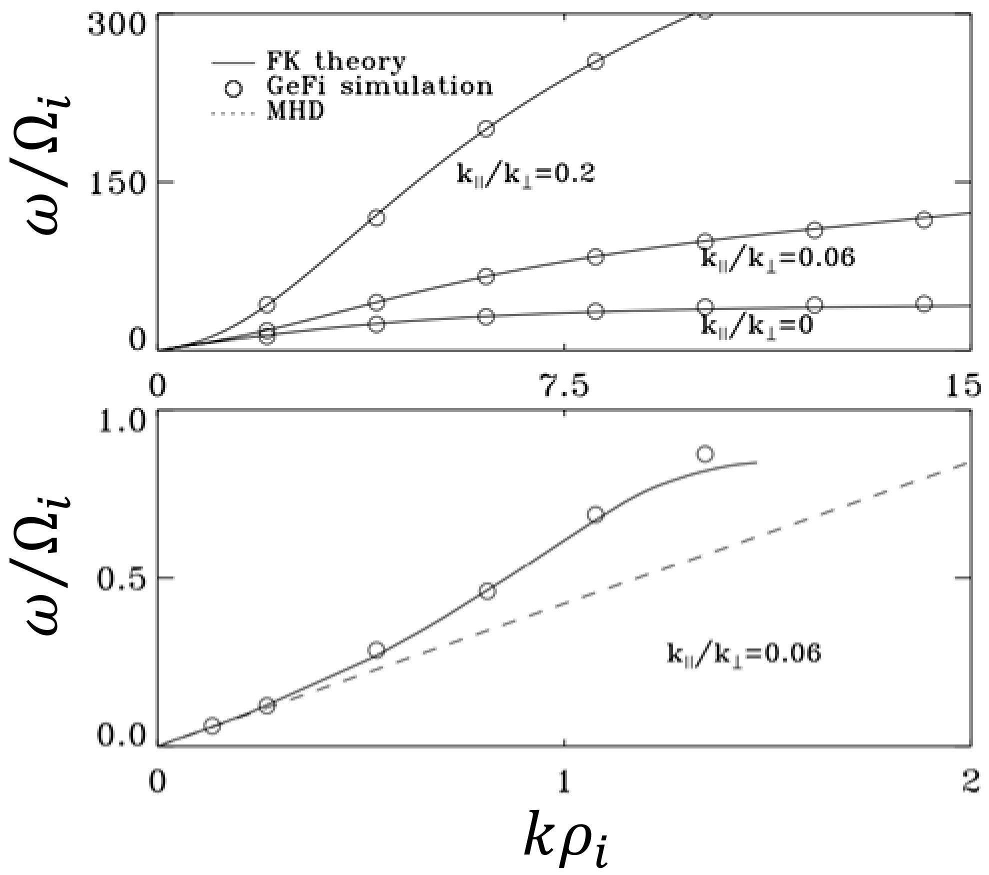

Lower-hybrid Brunch

Kinetic-Alfven Brunch

2.5 GeFi results vs. Explicit FK results

Explicit fully kinetic (FK) δf particle scheme

Particle equation of motion:

$$\frac{d\mathbf{v}_\alpha}{dt} = \frac{q_\alpha}{m_\alpha}\mathbf{v}_\alpha \times \mathbf{B}_0,$$
$$\frac{d\mathbf{x}_\alpha}{dt} = \mathbf{v}_\alpha.$$

Calculating distribution Function:

$$\frac{dW_\alpha}{dt} = -q_\alpha(\delta\mathbf{E} + \frac{\mathbf{v}_0}{c} \times \delta\mathbf{B}) \cdot \frac{\partial ln \bar{f}_\alpha}{\partial \mathbf{v}_\alpha},$$
$$W_\alpha = \delta f / \bar{f}_\alpha,$$

Field Calculation:

$$\nabla \times \delta\mathbf{E} = -\frac{1}{c}\frac{\partial}{\partial t}\delta\mathbf{B},$$
$$\nabla \times \delta\mathbf{B} = \frac{4\pi}{c}\delta\mathbf{J} + \frac{1}{c}\frac{\partial}{\partial t}\delta\mathbf{E},$$

Current deposition: $\delta\mathbf{J} = \int \mathbf{v}_\alpha \delta f_\alpha d^3\mathbf{v}_\alpha.$

Charge conservation: Solving Poisson's Equation in specific time-step

Lower-hybrid Waves in Uniform Plasmas

GeFi vs. FK explicit

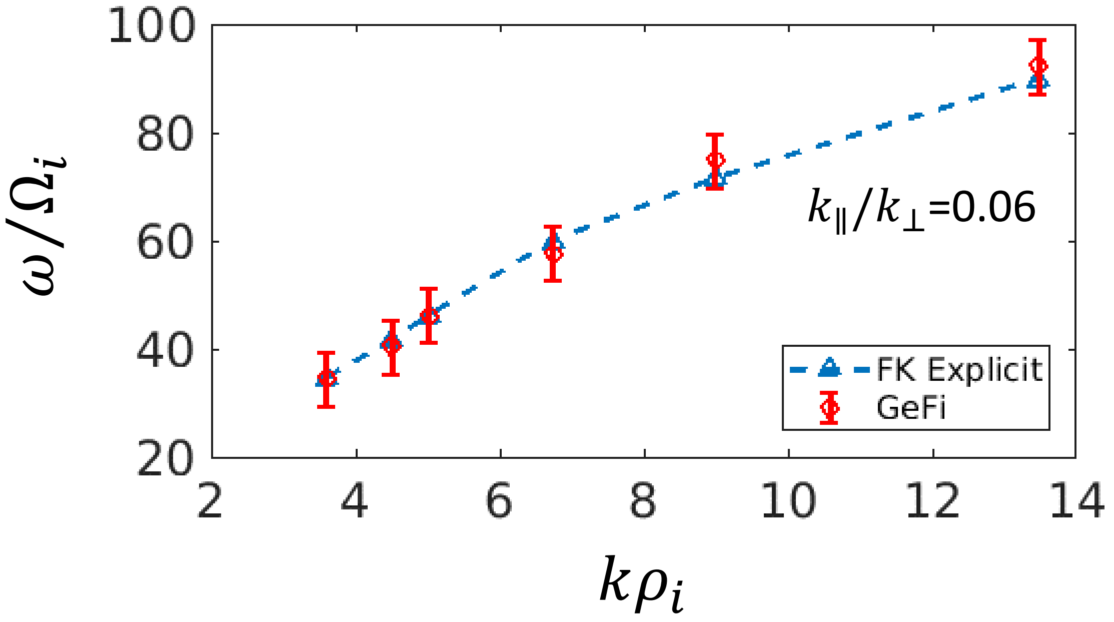

2.6 GeFi results vs. Darwin code results

Implicit fully kinetic Darwin full particle scheme [Neilson 1972, Swift 1986]

Darwin approximation: removes radiative terms while keeping charge conservation

Particle Hamiltonian equations of motion (implicit form):

$$\frac{d\mathbf{p}_j}{dt} = \frac{q_j}{m_j c}(\nabla \mathbf{A}) \cdot (\mathbf{p}_j - \frac{q_j}{c}\mathbf{A}) - q_j \nabla \phi \quad \text{(D.1)}$$

$$\frac{d\mathbf{x}_j}{dt} = \frac{1}{m_j}(\mathbf{p}_j - \frac{q_j}{c}\mathbf{A}) \quad \text{(D.2)}$$

Charge and Current Density:

$$\rho = \sum_{\alpha=i,e} q_\alpha n_\alpha \quad \text{(D.3)}$$

$$\mathbf{J} = \sum_{\alpha=i,e} \frac{q_\alpha}{m_\alpha} n_\alpha < \mathbf{p}_\alpha > -(\sum_{\alpha=i,e} \frac{q_\alpha^2}{m_\alpha c} n_\alpha)\mathbf{A} \quad \text{(D.4)}$$

$<\boldsymbol{p}_\alpha> = \Sigma_j \boldsymbol{p}_j \mathrm{S}(\boldsymbol{x} - \boldsymbol{x}_j)$ and $n_\alpha = \Sigma_j \mathrm{S}(\boldsymbol{x} - \boldsymbol{x}_j)$ are canonical momentum and density on grids.

Implicit fully kinetic Darwin full particle scheme

Insert ρ and $\mathbf{J}$ into EM field equation. Calculating the scalar and vector potential are

$$\nabla^2 \phi = -4\pi \sum_{\alpha=i,e} q_\alpha n_\alpha \tag{D.5}$$

$$\nabla^2 \mathbf{A} = -\frac{4\pi}{c} \sum_{\alpha=i,e} \frac{q_\alpha}{m_\alpha} n_\alpha < \mathbf{p}_\alpha > + \frac{4\pi}{c^2} \Big(\sum_{\alpha=i,e} \frac{q_\alpha^2}{m_\alpha} n_\alpha \Big) \mathbf{A} + \frac{1}{c} \nabla \Big(\frac{\partial \phi}{\partial t} \Big) \tag{D.6}$$

By using Coulomb gauge, $\frac{\partial \phi}{\partial t}$ can be obtained by

$$\nabla^2 \Big(\frac{\partial \phi}{\partial t} \Big) = 4\pi \sum_{\alpha=i,e} \nabla \cdot (n_\alpha < \mathbf{p}_\alpha >) - \frac{4\pi}{c} \Big(\sum_{\alpha} \frac{q_\alpha^2}{m_\alpha} \nabla n_\alpha \Big) \cdot \mathbf{A} \tag{D.7}$$

$\mathbf{A}$ and $\frac{\partial \phi}{\partial t}$ have to be simultaneously solved with (6) and (7) by iteration. The predictor-corrector method are used to solve the particle Hamiltonian equations of motion.

This model is suitable for problems with low frequencies ($\omega \lesssim \Omega_i$)

GeFi results and Darwin results from kinetic Alfven waves are consistent.

2.5 3-D current sheet

3-D geometry of Harris current sheet

Sheet normal: z

Anti-parallel magnetic field: B_{x0}
Guide field: B_G in y
Half-width of current sheet: L

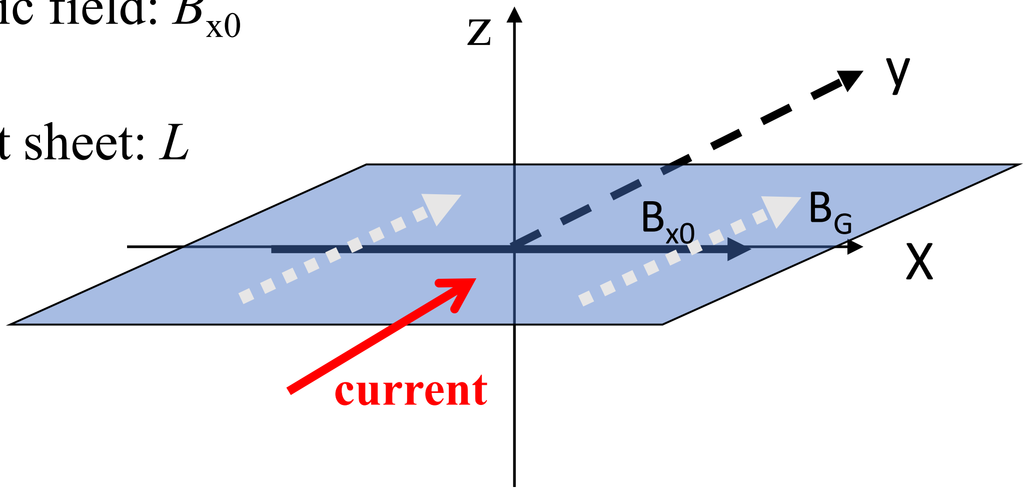

Validity of GeFi scheme in thin Harris current sheet:
$\rho_i \sim L$, ions must be treated as fully kinetic particle
$\rho_e \ll L$, electrons are still valid for GK approximation
$\omega \ll \Omega_e$, GeFi is particularly suitable to study current sheet!

Equilibrium in Harris current sheet

Ion distribution function:

$$\bar{f}_{Hi} = \frac{n_{h0}}{(2\pi T_i/m_i)^{3/2}} e^{-m_i\left[v_x^2+(v_y - V_{di})^2+v_z^2\right]/2T_i} \cdot e^{-V_{di}q_iA_y(z)/T_i}, \tag{19}$$

where $V_{di} = \frac{2q_e L(T_i+T_e)}{B_{x0}(1+T_i/T_e)}$ is ion drift speed and $n_{h0}e^{-V_{di}q_iA_y(z)/T_i} = n_{ih0}(z) = n_H \operatorname{sech}^2(z/L)$.

Electron distribution function in gyro-center coordinates:

$$\bar{F}_{He,g} = \frac{n_{ih0}}{(2\pi T_e/m_e)^{3/2}} \exp\left(-\frac{B_x^2}{B^2}\frac{m_e V_{de}^2}{2T_e}\right)\left(1 - \frac{m_e V_{de}}{T_e \Omega_e}\frac{dB_x}{dz}\mu\right) \times \exp\left\{-\frac{1}{2T_e}\left[2\mu B + m_e\left(v_\parallel - \frac{V_{de}B_G}{B}\right)^2\right]\right\}, \tag{20}$$

Simulation Setup

Current sheet: $\vec{B} = B_0 \tanh(z/L)\,\hat{x} + B_G\hat{y}$

Density profile: $n_i = n_H sech^2(z/L) + n_b$

Boundary condition: $\delta\boldsymbol{A} = \mathbf{0}$ and $\delta\phi = 0$

Ion-to-electron mass ratio $m_i/m_e = 459{\sim}1836$.

Grid number $N_x \times N_y \times N_z = 16 \times 16 \times 256$.

Particle number per cell is 100~1000 for both electrons and ions.

Time step $\Omega_e \Delta t = 0.5$.

$B_G/B_{x0} = 0.1{\sim}10$

Current sheet half-width $L = 0.25{\sim}\ 1.0\rho_{i0}$,

where ρ_{i0} is ion Lamor radius in the asymptotic region.

$\omega_{pe}/\Omega_{ce} = 1{\sim}10$, $\beta_{i0} = 0.033{\sim}0.16$, $T_e/T_i = 0.1{\sim}1$.

Because a GK model is, for the first time, used to study current sheet system, we compare every instability from GeFi simulation with the fully kinetic particle simulations.

4. Electrostatic simulation results

4.1 GeFi δf model in Electrostatic limit

Electrostatic GK Poisson's equation:

$$\left(1+\frac{\omega_{pe}^2}{\Omega_e^2}\right)\nabla_\perp^2\delta\phi = -4\pi(q_i n_i + q_e\langle N_e\rangle),$$

where $n_i = \int \delta f_i d^3v$ and $\langle N_e\rangle = \int \delta F_e d^3v$.

Next, show GeFi results in the 2-D out-of-plane plane, with comparison to FK simulations and GK eigen theory, and in the 3-D space.

2-D Electrostatic Simulation Results

m_i/m_e=1836, n_b=0, $L/\rho_{i0} = 0.23$, B_G/B_{x0}=0.1, $\omega_{pe}/\Omega_e = 1$, T_i/T_e=10

GeFi vs. FK:
Lower-hybrid-drift-instability

Real space structure

Eigen-mode Structure

Growth-rate

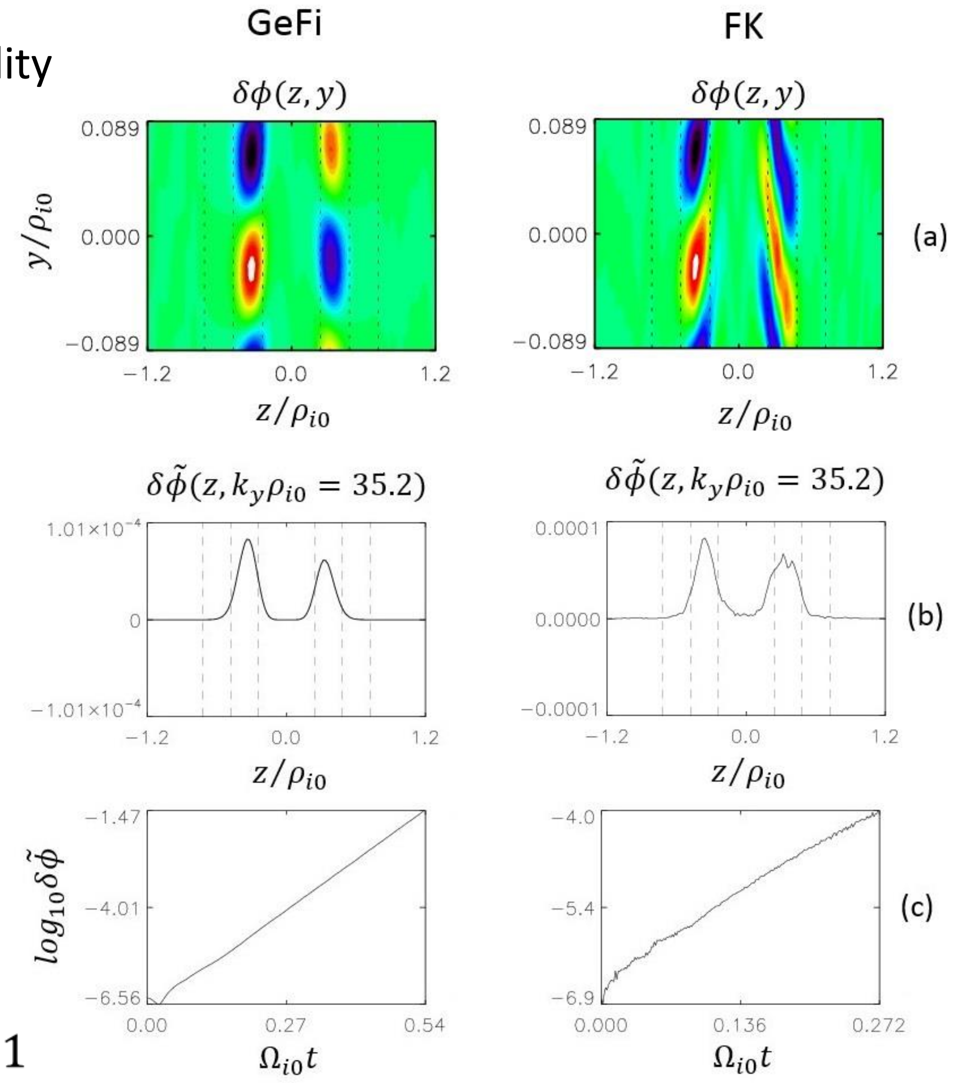

GeFi:

$\omega/\Omega_{i0} = 242.1$
$\gamma/\Omega_{i0} = 22.3$

FK:

$\omega/\Omega_{i0} = 230.7$
$\gamma/\Omega_{i0} = 21.1$

3-D Electrostatic LHDI : Growth-rate in the k_x-k_y space

$(m_i/m_e = 1836)$

k·B=0

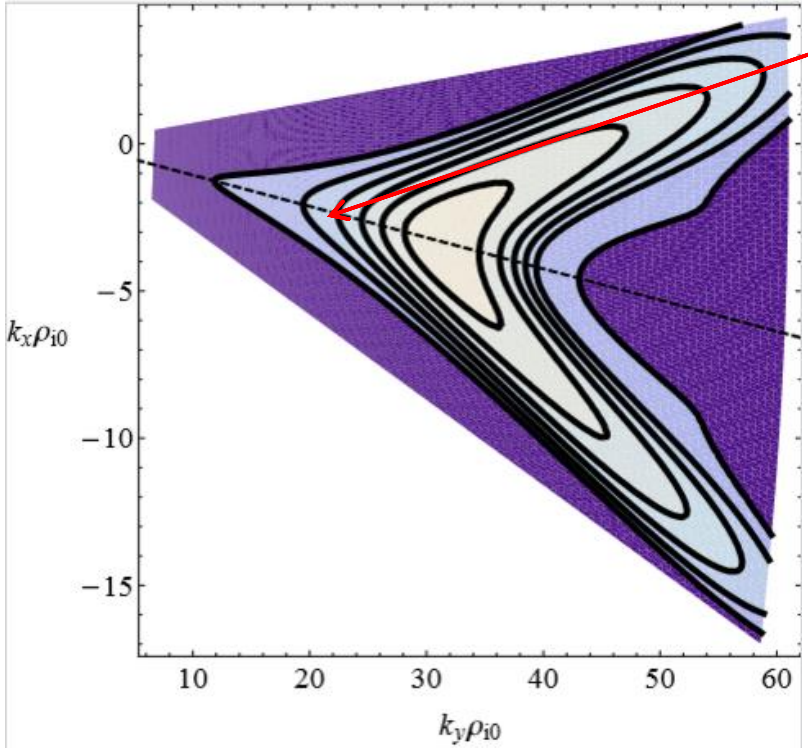

GeFi theory [*Tummel et al.*, 2015]

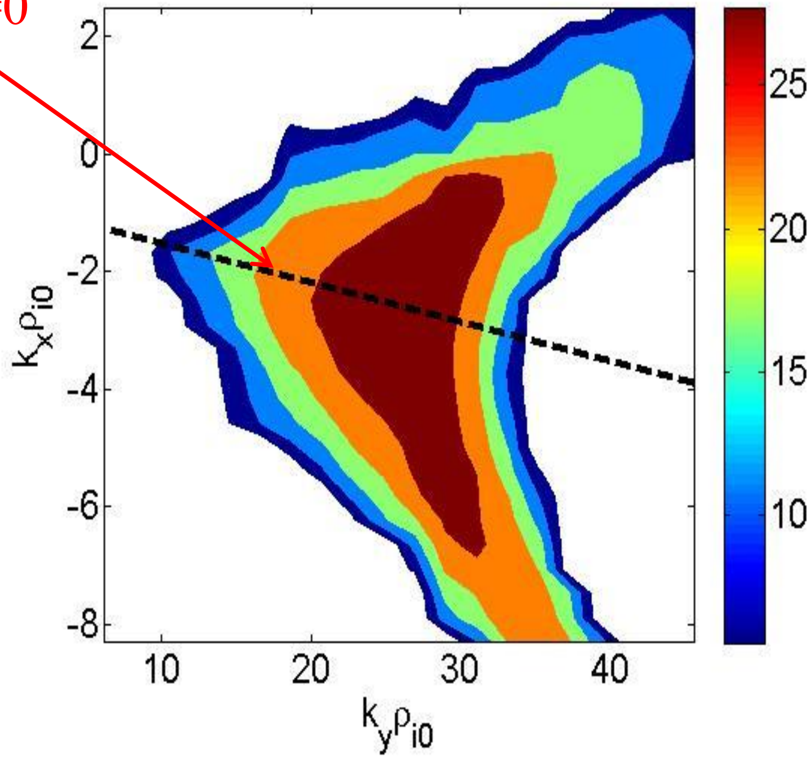

GeFi simulation

- Smaller k_y : LHDI peaks at **k**·**B** = 0, where **k**=(k_x, k_y).
- Larger k_y: (1) two peaks of LHDI; (2) the peaks are away from **k**·**B** = 0.

5. Electromagnetic Simulation results

5.1 2-D Results of LHDI (short wavelength)

m_i/m_e=1836, n_b=0, $L/\rho_{i0} = 0.23$, B_G/B_{x0}=0.1, $\omega_{pe}/\Omega_e = 1$, $k_y\rho_{i0}$=27.2

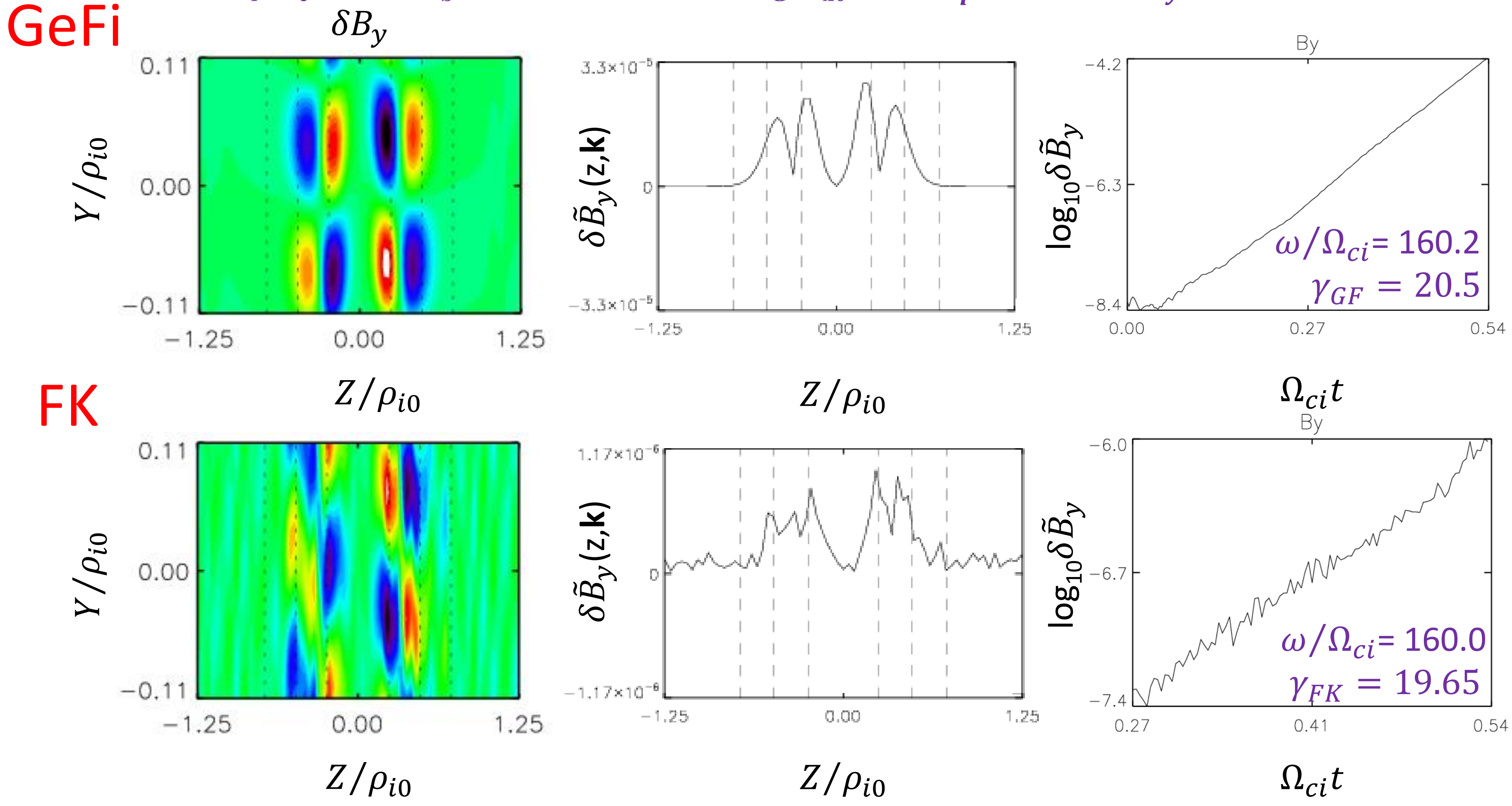

2-D Results of tearing mode instability in reconnection plane [Wang et al 2011]

B_{x0}/B_G=0.075, L/ρ_{s0}=1.5, T_i/T_e=1, k_xL =0.5, m_i/m_e = 1836.

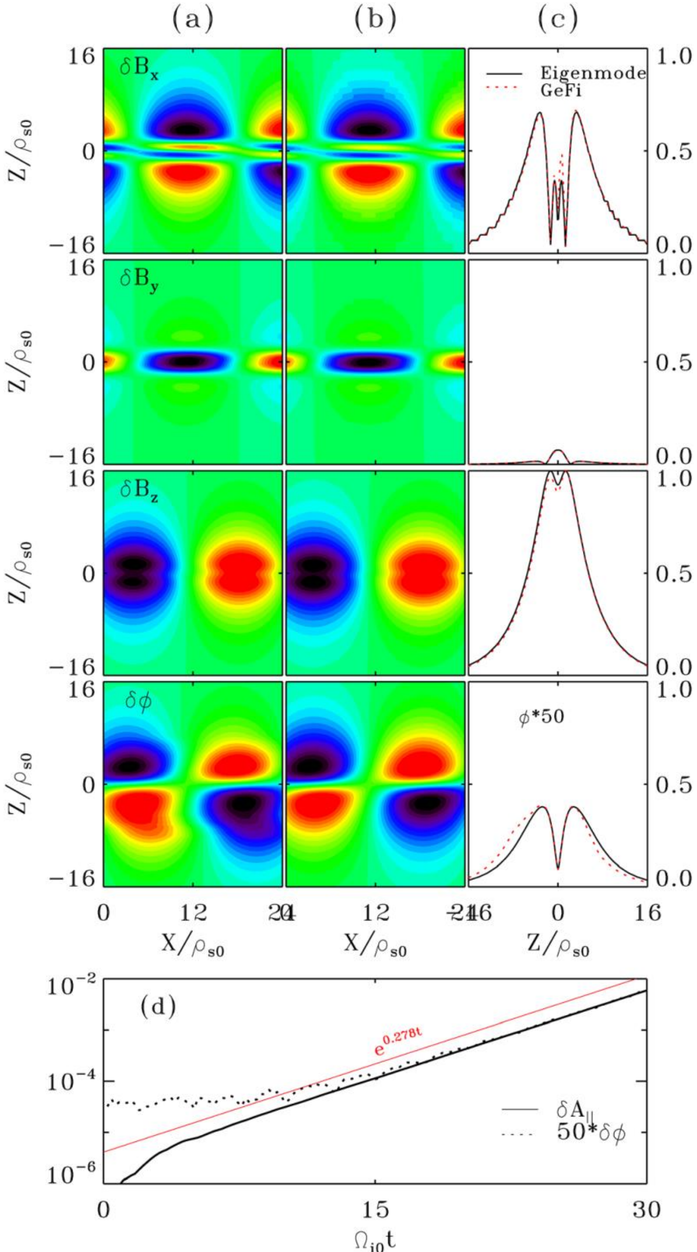

(a) GeFi results
(b) FK Darwin results
(c) Eigenmode structure
(d) Linear growth

3-D EM Kink instability: GeFi vs FK

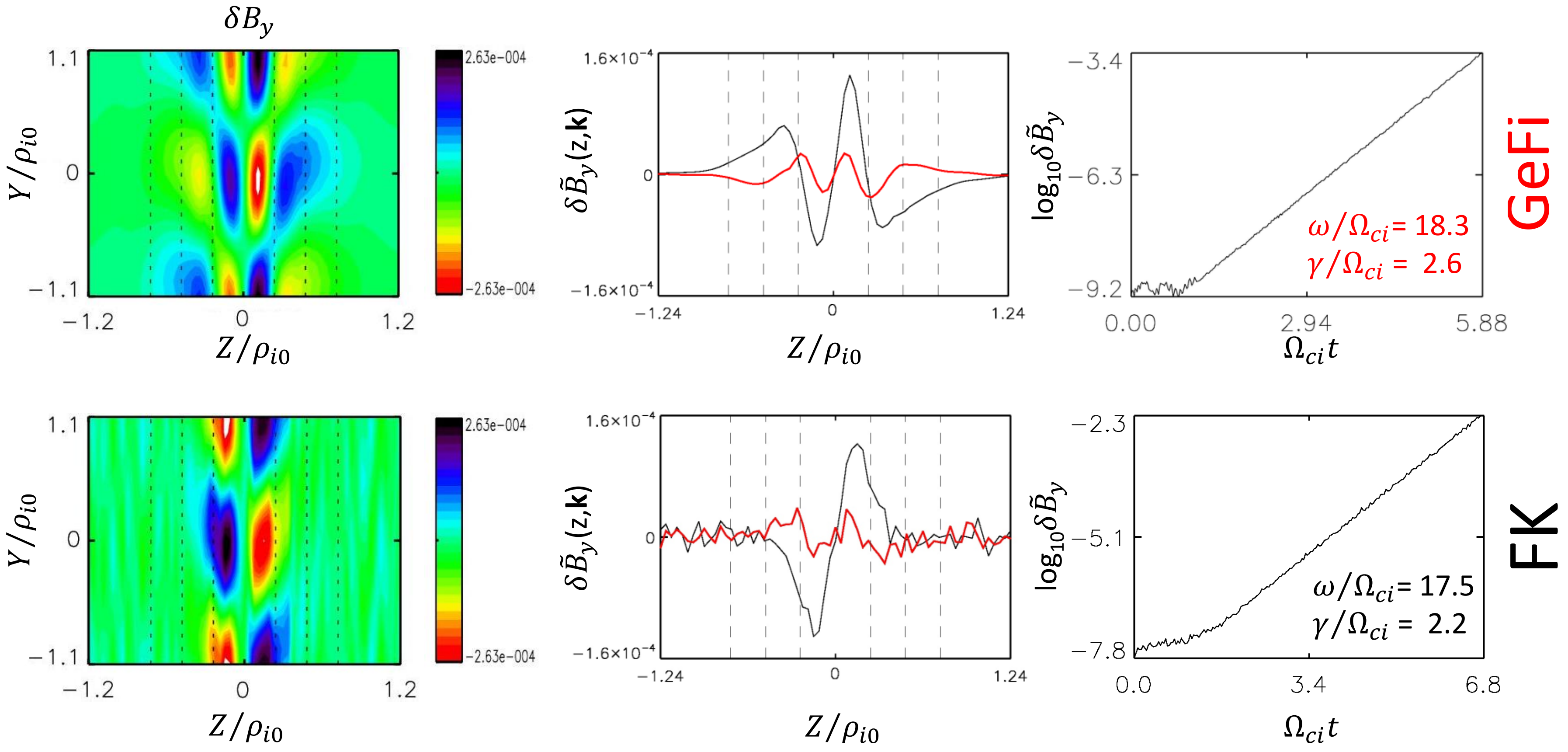

m_i/m_e=1836, n_b=0, $L/\rho_{i0} = 0.25$, B_G/B_{x0}=0.3, $\omega_{pe}/\Omega_e = 1$,
$k_y\rho_{i0} = 2.8$, $k_x\rho_{i0} = 0.4$ (GeFi) and $k_x\rho_{i0} = 0$ (FK)

3-D EM Sausage instability: GeFi vs FK

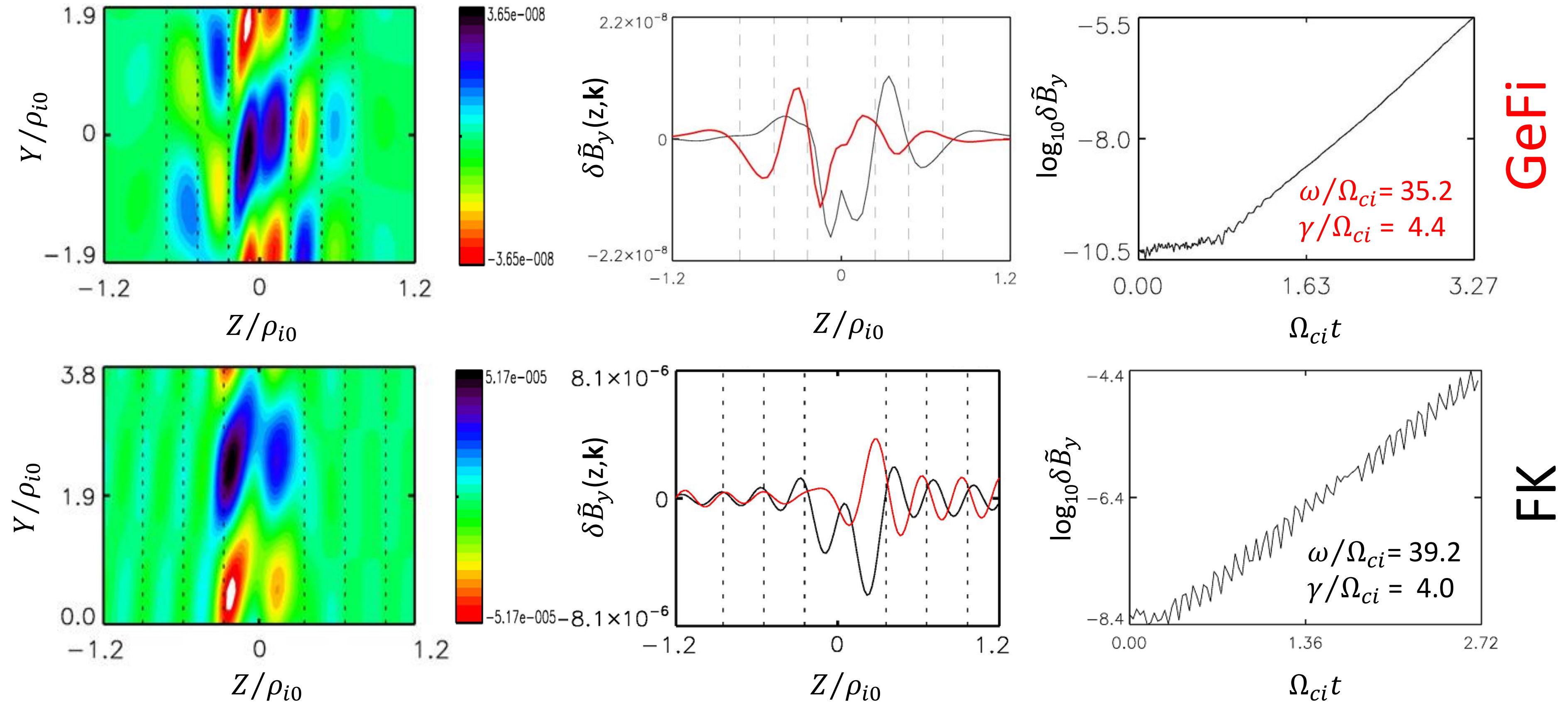

m_i/m_e=1836, n_b=0, $L/\rho_{i0} = 0.25$, B_G/B_{x0}=0.2, $\omega_{pe}/\Omega_e = 1$,
$k_y\rho_{i0} = 5.2$, $k_x\rho_{i0} = 2.4$ (FK) and $k_x\rho_{i0} = 0.8$ (GeFi)

Growth rate contours of 3-D Kink and Sausage Instabilities

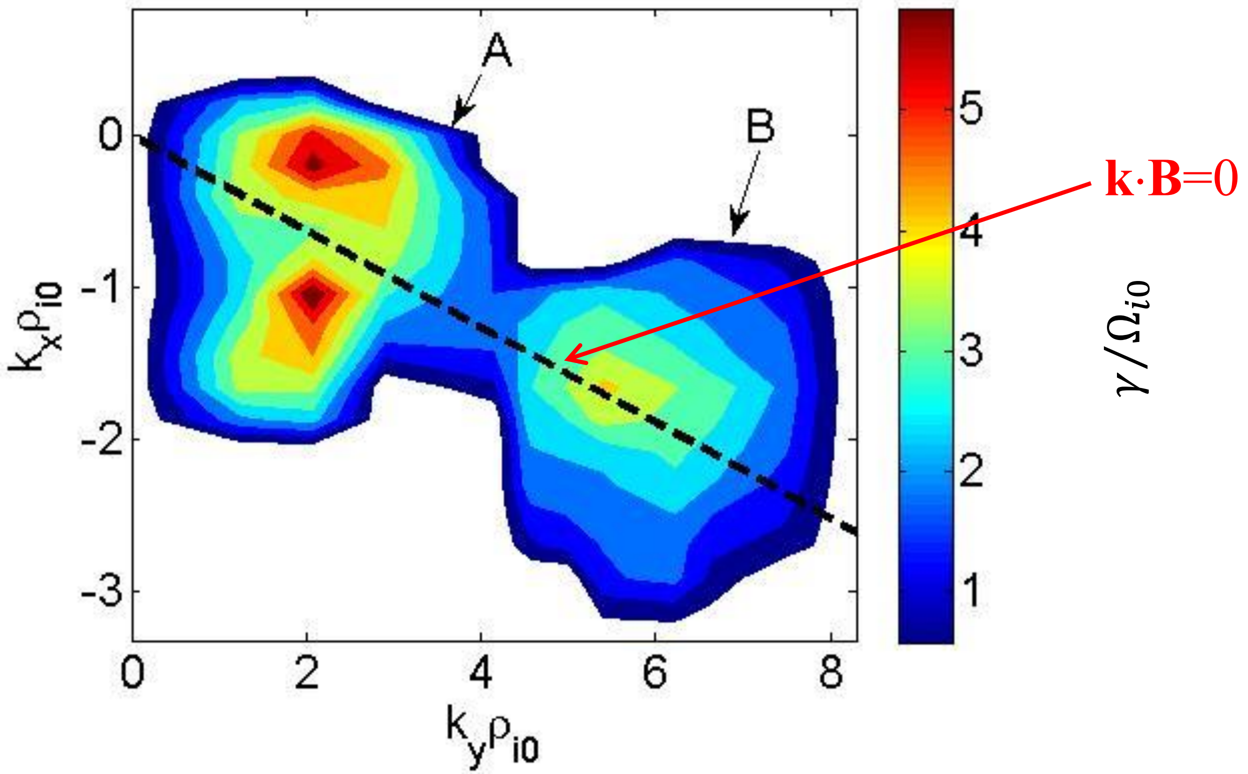

A: kink instability

B: sausage instability

EM Nonlinear results of Lower Hybrid Drift Instability: GeFi vs. Fully kinetic PIC

[VPIC, Daughton 2004]

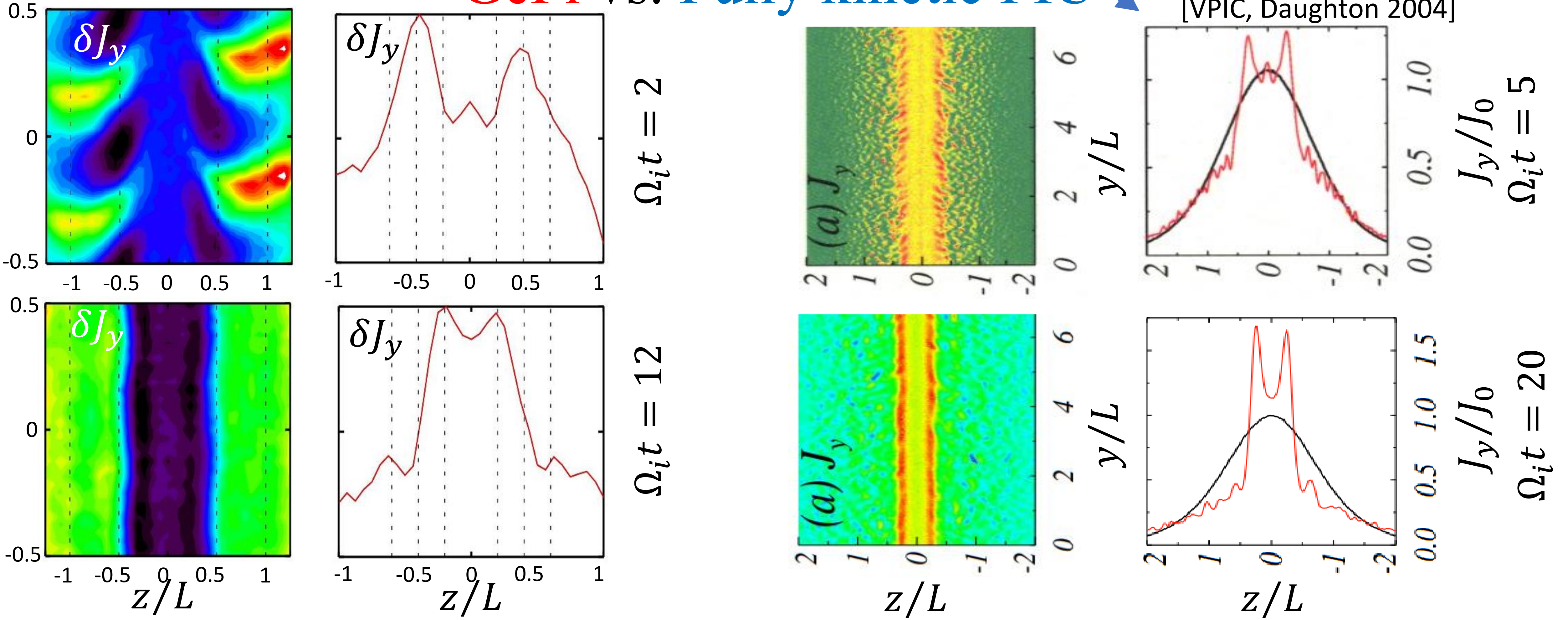

GeFi simulation shows δJ moving toward the center, consistent with fully kinetic PIC results!

EM Nonlinear δf results of Lower Hybrid Drift Instability:

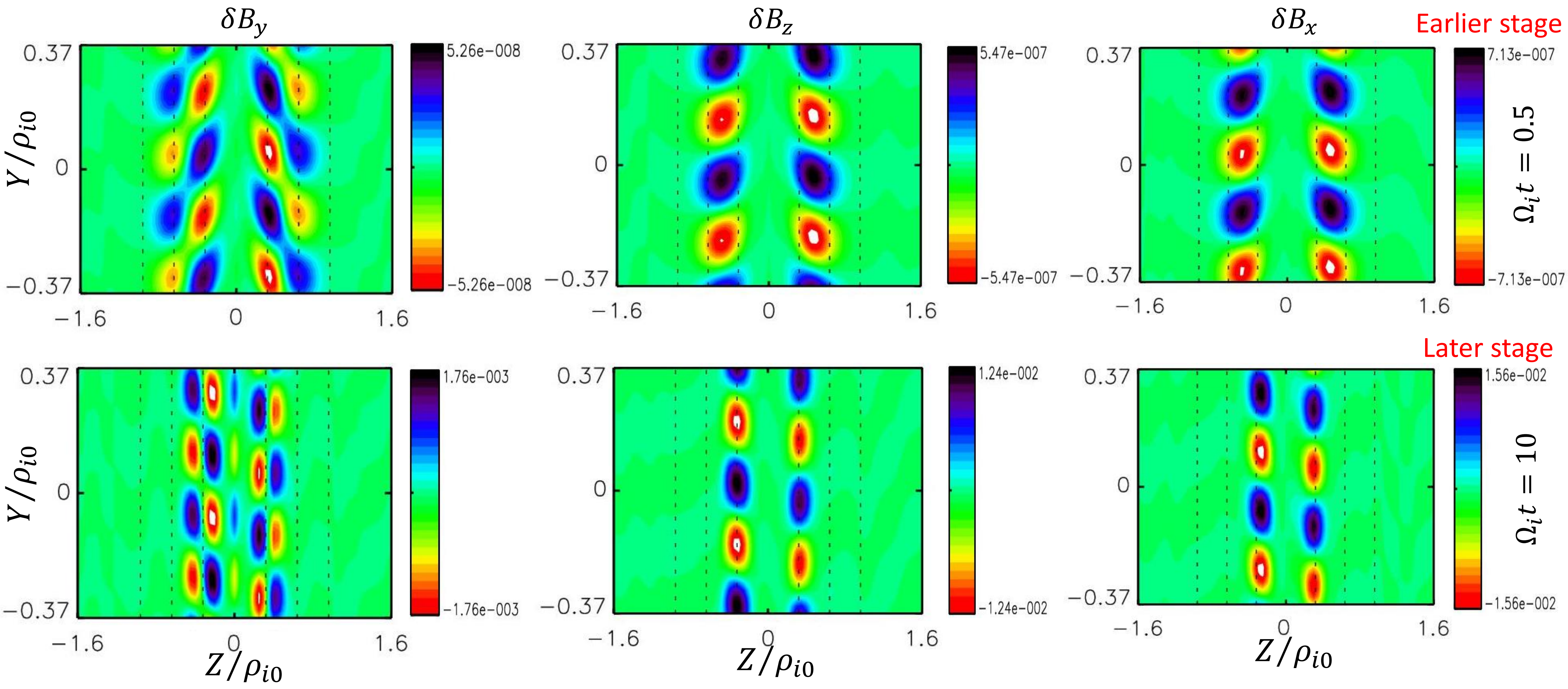

The nonlinear simulations show $\boldsymbol{\delta B}$ penetrate into the center region of current sheet

6. Summary

- In this talk, the gyrokinetic electron and fully kinetic ion particle (GeFi) simulation scheme is described.
- To validate the GeFi scheme and code, the results from Gyrokinetic electron and Fully kinetic ion (GeFi) code are compared with the results from the fully kinetic particle codes in cases of kinetic Alfven waves and lower hybrid waves.
- 3-D GeFi particle simulation scheme is used to investigate the current sheet instabilities, under a finite guide field B_G and the realistic mass ratio m_i/m_e.
- GeFi simulations have found two new current sheet instabilities (kink and sausage) in lower-hybrid-frequency range. These new instabilities are also found in the FK δf particle simulations. In nonlinear stage, the GeFi results are consistent with the FK results in case of tearing mode and LHDI.